# DEVELOPMENT AND CHARACTERIZATION OF HELICAL PASSAGE PRESSURE-SWIRL ATOMIZER

by

**Palash Barman**



DEPARTMENT OF AEROSPACE ENGINEERING

**Indian Institute of Technology Kanpur**

DECEMBER, 2002

# DEVELOPMENT AND CHARACTERIZATION OF HELICAL PASSAGE PRESSURE- SWIRL ATOMIZER

A Thesis submitted
In Partial Fulfillment of the Requirements
For the degree of

**MASTER OF TECHNOLOGY**

**By**

**PALASH BARMAN**

To the

**DEPARTMENT OF AEROSPACE ENGINEERING**

## INDIAN INSTITUTE OF TECHNOLOGY KANPUR

Dec, 2002

# CERTIFICATE

This is to certify that the investigation on **'DEVELOPMENT AND CHARACTERIZATION OF HELICAL PASSAGE PRESSURE-SWIRL ATOMIZER'** has been carried out by **MR. PALASH BARMAN** under my guidance and it has not been submitted elsewhere for a degree.

Dr. Abhijit Kushari
Assistant Professor
Department of Aerospace Engineering
Indian Institute of Technology Kanpur

# DEDICATION

*Dedicated*
*to*
*My parents and beloved Shravasti*

# ACKNOWLEDGEMENT

At the outset I would like to convey my deepest sense of gratitude to my thesis supervisor **Asst. Prof. A. Kushari** without whose support, inspiration, prudence, able guidance it could never have been completed.

I would like to convey my sincere thanks to Mr. Bikas Mandal and Mr. Rawat and Mr. D.Patnaik for extending all possible and sincere help.

Finally I would like to mention those integral part of my IIT life, my friends, who have made every moment of stay here at IITK to rejoice in future.

PALASH BARMAN

December, 2002

IIT Kanpu

# CONTENTS


| | |
|---|---|
| Title Page | i |
| Certificate | ii |
| Dedication | iii |
| Acknowledgements | iv |
| Contents | v |
| List of Tables | vii |
| List of Figures | viii |
| Nomenclature | x |
| Abstract | xii |
| Chapter I: Introduction | 1 |
| 1.1 Need for atomization | 3 |
| 1.2 Brief discussion of atomizer | 3 |
| 1.2.1 Pressure atomizer | 4 |
| 1.2.2 Rotary atomizer | 4 |
| 1.2.3 Air blast atomizer | 5 |
| 1.2.4 Effervescent atomizer | 5 |
| 1.2.5 Internally mixed air assisted atomizer | 6 |
| 1.3 Theory of droplet formation | 11 |
| 1.4 Theory of droplet disintegration | 15 |
| Chapter II: Theoretical study of helical passage pressure-swirl atomizer | 18 |
| 2.1 Flow in the atomizer | 18 |
| 2.1.1 Spray cone angle | 21 |
| 2.2 Air core | 27 |

Chapter III: Atomizer design 29

3.1 Design procedure 29

3.2 Effect of various parameters on the performance of atomizer 37

Chapter IV: Experimental study of helical passage pressure-swirl atomizer 39

4.2 Design of test rig 39

4.2.1 Design of pressurized container 40

4.2.2 Thickness of the tube 41

4.2.3 Rotameter 41

4.2 Rotameter calibration procedures 41

Chapter V: Evolution of spray in pressure-swirl atomizer 47

5.1 Experimental effort 48

5.2 Effect of supply pressure 48

Chapter VI: Conclusion 64

# LIST OF TABLES

Table A: Classification of jet breakup regimes [7] 12

# LIST OF FIGURES


| Figure | | Page |
|---|---|---|
| 1.1 | Schematics of pressure atomizers [3] | 8 |
| 1.2 | A schematic of a rotary atomizer [3] | 8 |
| 1.3 | A schematic of an air-blast atomizer [3] | 9 |
| 1.4 | A schematic of an effervescent atomizer | 10 |
| 1.5 | A schematic of an internally mixed atomizer [3] | 10 |
| 1.6 | Liquid jet Disruption [11] | 13 |
| 2.1 | Dependence of $C_D$ with non-dimensional geometric characteristic | 24 |
| 2.2 | Dependence of $\alpha$ with non-dimensional geometric characteristics ($A_S$) | 25 |
| 2.3 | Dependence of $\phi$ with non-dimensional geometric characteristics ($A_S$) | 26 |
| 2.4 | Development of air core in pressure-swirl Atomizer | 28 |
| 3.1 | Schematic diagram of Injector designed | 36 |
| 4.1 | Schematic diagrams for rotameter calibration | 43 |
| 4.2 | Water flow rate (lit/min.) vs. Rotameter scale reading | 44 |
| 4.3 | Schematic diagram of experimental setup | 46 |
| 5.1 | Evolution of spray in pressure-swirl Atomizer | 51 |
| 5.2 | Dependence of velocity on pressure | 56 |
| 5.3 | Dependence of Reynolds number ( $R_e = \frac{\rho V d_2}{\mu}$ ) on pressure | 56 |
| 5.4 | Dependence of Co-efficient of discharge ($C_{da}$) on non-dimensional pressure | 57 |
| 5.5 | Dependence of Reynolds number on the actual co-efficient of discharge ($C_{da}$) | 58 |
| 5.6 | Dependence of spray angle on Reynolds's number | 59 |
| 5.7 | Dependence of Weber number ($W_e$) on velocity | 60 |
| 5.8 | Dependence of Weber number ($W_e$) on non-dimensional pressure | 61 |
| 5.9 | Dependence of non-dimensional break up length on | |

non-dimensional pressure 62

5.10 Dependence of non-dimensional break up length on Gas Weber number 63

# NOMENCLATURE

| | |
|---|---|
| $a$ | Width of the helical passage at inner radius |
| $a_2$ | Cross sectional radius of orifice |
| $A_H$ | Cross sectional area of helical passage |
| $A_S$ | Non-dimensional geometric characteristics |
| $b$ | Width of the helical passage at the outer radius |
| $c$ | Constant |
| $C_D$ | Fictitious co-efficient of discharge |
| $C_{da}$ | Experimental coefficient of discharge |
| $d_1$ | Outer diameter of the screwed element |
| $d_2$ | Diameter of the orifice |
| $d_H$ | Equivalent diameter of the helical passage |
| $f_A$ | Friction factor at the inlet |
| $f_H$ | Friction factor through helical passage |
| $f_{ST}$ | Friction factor for straight injector |
| $g$ | Acceleration due to gravity |
| $h$ | Height of the helical passage |
| $L$ | Total length of the injector |
| $l/d_2$ | Non-dimensional breakup length |
| $n$ | Number of ports |
| $N$ | Number of turns |
| $P_{atm}$ | Atmospheric pressure |
| $P_1$ | Driving pressure |
| $Q$ | Volumetric flow rate of water |
| $r$ | Any radius in the orifice |
| $R$ | Mean radius of the helical passage |
| $r_a$ | Air core radius |
| $R_e$ | Reynold's number |
| $R_{eH}$ | Reynold's number through helical passage |
| $t$ | Thickness of the injector |

| | |
|---|---|
| $t_{th}$ | Theoretical thickness |
| $u_2$ | Axial velocity through the orifice |
| v | Tangential velocity at any radius in the orifice |
| $V_2$ | Tangential velocity in the orifice |
| $v_2$ | Tangential velocity through the orifice |
| $V_A$ | Axial velocity |
| $V_R$ | Resultant velocity through helical passage. |
| $V_t$ | Tangential velocity |
| $W_e$ | Weber number |
| $\pi$ | 3.141 |
| $\varphi$ | Area coefficient (flow area / orifice area) |
| $\theta$ | Convergence angle |
| $\beta$ | Helix angle |
| $\tau$ | Pitch of the helix |
| $\alpha$ | Spray cone angle |
| $\gamma$ | Surface tension |
| $\mu$ | Viscosity of water |
| $\rho$ | Density of water |
| $\Delta P$ | Pressure difference |
| $\Delta P_A$ | Pressure drop at the inlet section due to friction |
| $\Delta P_H$ | Pressure drop through helical passage due to friction |
| $\Delta P_W$ | Pressure drop in the orifice |

# ABSTRACT

A pressure-swirl liquid atomizer with helical internal passage was designed fabricated and characterized. Helical passage was provided to impart a tangential velocity component to the liquid flow. The liquid turns in the settling chamber and exits the atomizer with a radial and tangential velocity component along with the axial velocity. This leads to the formation of a conical liquid sheet, which subsequently breaks into ligaments and droplets. The dependence of the jet break up length and spray angle on the liquid supply pressure was studied using flow visualization technique. It was seen that the spray angle increases with supply pressure and then become constant. The break up length first decreases and then increases and again decreases owing to different aerodynamic and surface tension forces.

# CHAPTER I

## Introduction

Atomizer plays a very important role in the performance of liquid rocket engines. For combustion of liquid propellants in the minimum chamber volume, atomizer should provide uniform distribution of propellants in the chamber cross-section both in terms of component ratio and in terms of flow-intensity. The size of the droplets fed to the chamber should be as uniform as possible and should be sufficiently small, so that simultaneously the process of their evaporation would be completed faster. Mutual location of the fuel as well as oxidizer injectors and their hydraulic parameters (Weber number, Reinhold's number, Nusselt's number, Strouhal number etc.) should give rise not only to uniform distribution of propellants, but also active heat addition from the combustion chamber to atomized propellants for its rapid evaporation and promote creation of conditions in the chamber for intense mixing of propellant components. In a nutshell, the main functions of atomizer are as follows:

1 To introduce the propellant with desired F/O ratio into the combustion chamber.

2 To cause the necessary degree of liquid mixing or interpenetration plus atomization, or both in order to achieve rapid and complete mixing.

3 To distribute the propellant spray uniformly in the combustion space to make the combustion as compact as possible.

4 To provide proper pressure drop to fix the flow ratio and to dampen the disturbances.

The transformation or break up of liquid fuel into a spray is of great importance in liquid fuel combustion that is used in various propulsion systems and industrials

processes. The spray, comprising of a multitude of droplets, provides a much larger surface area compared to the bulk liquid, thus greatly enhancing the liquid evaporation rate. Numerous spraying devices, which operate on different principles and are broadly designated as atomizers or injector, have been developed over the years. The liquid atomization, process contains two stages, primary atomization and secondary atomization. Primary atomization refers to droplet disintegration from a continuous liquid body. Secondary atomization refers to further droplet break up or coalescence with other droplets during the transport process. Most studies in the past have been combined these two processes and treated them as one global process. For example, Rizk and Lefebvre [1] Suyari and Lefebvre [2], Wang and Lefebvre [3] and others have illustrated those liquid properties of viscosity, surface tension and density influence on atomization quality. However, to better understand the atomization mechanism, it is important to examine separately the two above mentioned atomization quality. Our investigation is focused on the primary atomization stage of a simplex pressure –swirl spray and, specifically to investigate experimentally the effect pressure on conical liquid sheet disintegration.

The phenomenon of liquid sheet disintegration has been extensively studied theoretically. In the theoretical analysis, it has been concluded that Weber number (ratio of inertia and interfacial surface tension forces) is an important parameter for liquid break up and Ohneshorge number (ratio of internal viscous force to the interfacial surface tension force) is also an important factor if liquid viscosity is considered. The effect of Reynolds number is not explicitly discussed.

In our study, the liquid sheet break up length is not only found to be a function of Weber number but a function of Reynolds number. Apart from this, this study examines quantitatively the effect of supply pressure on discharge co-efficient, break up length and spray angle of a simplex pressure swirl injector. Discharge coefficient specifies the available flow rate of the injector and also indicates the pressure loss across the injector. Break up length represents the liquid disintegration potential of the injector. Qualitatively liquid sheet features, that is, the sheet appearance and the spray cone shape, illustrate the spray development and relate to the atomization quality. Such studies can help one

understand how an atomizer handles fluid, so that one can maintain atomizer spray quality.

## 1.1 Need for atomization

The combustion of liquid fuels involves atomization of a bulk liquid into a multitude of droplets, thus increasing the liquid surface area and enhancing the rate of evaporation of liquid fuel. The formed fuel vapor then mixes with the air to form a combustible mixer. Therefore, the evaporation time, along with the mixing time and chemical reaction time, play a very important role in the performance of liquid-fueled combustion devices, which, in turn, depends on the sizes of the generated droplets.

The quality of combustion processes, e.g., ignition, flame stability, efficiency, combustion stability and emission levels, in liquid-fueled engines strongly depend on the quality of the fuel spray [4, 5, 6]. There is evidence [4, 5] that the performance of the combustion process under a given operating condition may be optimized by generating a spray with a specific mean droplet size, which may not be the minimum size that could be generated by the atomizer. Fine atomization causes substantial reduction in the production of unburned hydrocarbons because it reduces the evaporation time of the droplets and, thus, improves mixing and increases the time available to attain complete combustion [5]. Complete combustion caused by finer atomization leads to a decrease in soot formation. Finer atomization also improves the combustion efficiency by reducing evaporation time [4]. On the other hand, the reduction in mean droplet size increases the emission of NOx. This can be attributed to the reduction in evaporation time and consequent increase in the time spent by the combustion products in the combustion zone, thus increasing the time available for NOx production reaction to proceed towards equilibrium [5]. Furthermore, finer atomization reduces the lean blow out limit of the engine because of the decrease in the evaporation time [4]. Therefore, it could be possible to optimize the combustion process and reduces emission by using pressure-swirl by operating it at a pressure higher than pressure at which air core is fully developed.

## 1.2 Brief discussion of Atomizer

Atomizer is often accomplished by discharging the liquid at a high velocity into a relatively slow-moving steam of air or gas or by destabilizing the liquid column using mechanical devices. In this section, the general features of various types of atomizers are described.

### 1.2.1 Pressure Atomizer

As their name suggests, pressure atomizers rely on the conversion of pressure energy into kinetic energy to achieve a high relative velocity between the liquid and the surrounding gas. Most of the atomizers in general use are of this type. They include plain-orifice and simplex nozzles, as well as variable geometry, duplex and dual orifice injectors [3, 7]. The schematics of various types of pressure atomizers are presented in Fig.1.1. Disintegration of liquid jet, emerging from pressure atomizers, is promoted by an increase in flow velocity, which enhances both the level of turbulence in the liquid jet and the aerodynamics drag forces exerted by the surrounding medium [3, 7]. In simplex or pressure atomizers, a swirling motion is imparted to the liquid so that, under the action of centrifugal force, it spread out in the form of a conical sheet as soon as it leaves the orifice. This sheet then breaks up into liquid droplets under the influence the external and internal forces. Since the flow rates and droplet sizes obtained from the pressure atomizers depend on the pressure drop across the injector, the quality of atomization is very poor at low flow rates causing very unsatisfactory combustion. The lower limit of this flow rates depends on the atomizer design. At high flow rates the operating pressure are very high, e.g. in the range 100psi. Thus, poor atomization at low flow rates and high operating pressure at high flow rates bound the range of operation of pressure atomizers. Furthermore, since the fuel rates and droplet sizes are directly related to each other through the operating pressure, these two parameters cannot be controlled independent of each other.

### 1.2.2 Rotary Atomizer

In then rotary atomizers [3, 7], liquid is supplied through stationary tube to the inner port of the rotating surface as shown in the Fig.1.2. The friction between the liquid and the rotating surface causes the liquid to rotate with the surface and the centrifugal force cause s it to flow towards the periphery. Under the action of this centrifugal force,

the liquid leaves the edge of the surface with high velocity, producing a fine spray. In rotary atomizers, even high flow rates of liquid can be atomized with relatively low pressure. They can be clean readily and display minimal flow blockage. However, the design is very complex, including a rotating element with the accompanying transmission and lubrication systems. They require high rotational speed of the surface to achieve good quality of atomization. Such high speed reduces the reliability and require appropriate protections.

### 1.2.3 Air Blast Atomizer

The drive to improve the generated sprays has resulted in an increase in the use of air blast atomizers [3, 7] in modern engines. In such injectors blasting of liquid sheets and ligaments by slow-moving, high-pressure air from the compressor induces atomization. However, due to the small pressure drop between the compressor discharge and the combustor, kinetic energy of the blasting air is limited. Therefore, they require large quantities of air (typically 500 to 600 percent of liquid Mass.) to attain satisfactory atomization. But, this additional air is not wasted, because, after atomizing the fuel it conveys the drops into the combustion zone and also supplies a fraction of the primary combustion air. A schematic diagram of an air-blasted atomizer is presented in Fig.1.3

Air blasted atomizer have many advantages over pressure atomizers. They require lower fuel pump pressure and produce finer sprays. The atomization process ensures very good mixing of air and fuel, reducing soot formation. The main advantage of air blast atomizers is that the large quantities of atomizing air required by these injectors are not available during start up of the engines, idling and high altitude flight, resulting in poor sprays and the combustion processes at those off- design operating condition. Furthermore, the "drowning" and blasting of liquid jet by huge quantities of air leaves very little room for any mind of control of the atomization process [3, 7].

### 1.2.4 Effervescent Atomizer

In effervescent atomizers [6, 7, 8, 9], a small amount of air or gas is introduced into the bulk liquid in a mixing chamber upstream of the discharge orifice, as shown in Fig.1.4. The injected gas forms a bubbly two-phase, gas-liquid flow when it mixes with the liquid in the mixing chamber inside the injector. When the gas bubbles emerge from

the injector they "explode". This rapid expansion of the gas bubbles shatters the surrounding liquid ligaments, resulting in the formation of very fine droplets. Quantity of atomization obtained from effervescent atomizers is very good even at very low injection pressure. They have large holes and passages and can thus atomize "dirty" fuels without plugging the injectors. These injectors are reliable, simple and cheap. However, Effervescent atomizers are sensitive to acceleration owing to the sensitivity of air bubbles to acceleration. Consequently, they cannot be safely employed in airborne applications.

### 1.2.5 Internally Mixed Air Assisted Atomizer

In internally mixed, air assisted, atomizers the atomizing air interacts with the liquids inside the injector and assist in the atomization process [3, 7, 10, 11, and 12]. It is believed that two effects induce atomization in an internally mixed atomizer. First, as both the liquid and the atomizing air share the same flow passage inside the injector, the liquid is restricted to a smaller available flow area. The reduction in flow area accelerates the liquid and, thus, increases its kinetic energy. This increase in the kinetic energy of the liquid induces fine atomization. Second, the relative motion between gaseous and liquid phases produces a shear force at their interface. This force strips liquid droplets from the liquid filaments and thus, induces atomization. Since most of the atomizing energy is supplied by the atomizing air, this injector requires a very small pressure drop of liquid across the injector to produce fine spray, in contrast to the large pressure drop required in pressure atomizer, furthermore, internally mixed atomizer need a significantly lower flow rate of atomizing air compared to air blast atomizer. An atomizing air flow rate of only 10 to 20 percent of the liquid flow rate (by mass) can produce very fine atomization. Therefore, the internally mixed injector appears attractive for airborne gas turbine applications, as it requires small amount of atomizing air to produce fine atomization with only a small liquid pressure drop across the injector. A schematic of an internally mixed, air-assisted atomizer is presented in Fig.1.5. The disadvantage of the injector is that it requires additional compression of the atomizing air. It is envisioned that in airborne engine application this injector will obtains its air from a small, electrically driven, auxiliary compressor that will compress a small fraction of the main compressor air, e.g., 0.5 percent of total air flow rate by about 50 psi.

Conceptually, internally mixed atomizers are similar to effervescent atomizers. However, instead of forming a bubbly air liquid mixer inside the injector, a low flow rate of pressurized air is impinged upon the liquid, a short distance upstream of the injector's orifice exit in an internally mixed atomizer. Since the interaction between air and liquid occur over a very short distance, eliminating the possibilities of bubble formation [8], the resulting atomization process is expected to be less sensitive acceleration.

Another potential advantage of internally mixed atomizer is choking of the two phase flow of liquid and air as it passes through the injector, due to low sonic velocity of two phase liquid air mixture [11]. Therefore, the liquid flow rate is relatively insensitive to the variation in the combustion chamber pressure and, thus, the fuel flow rate is not likely to respond to combustor disturbances, which will reduce the likelihood of combustion instabilities by reducing the coupling of combustor pressure and fuel flow oscillations.

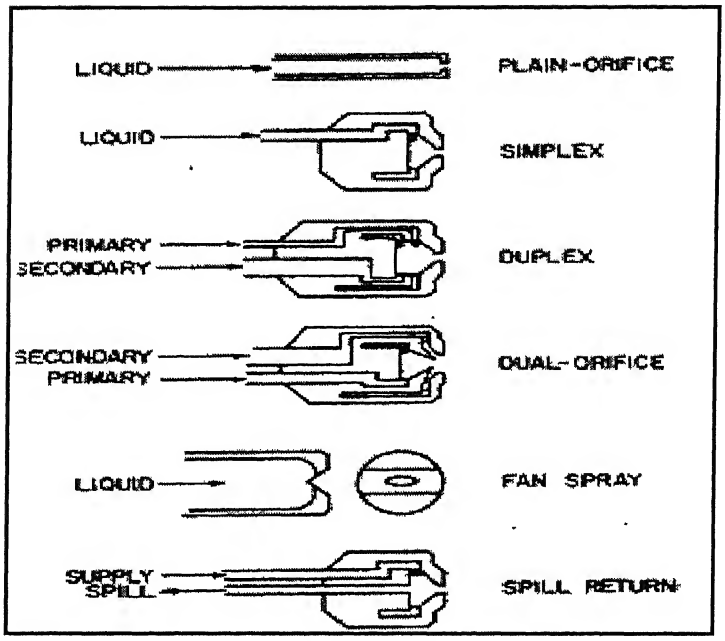


Figure 1.1: Schematics of pressure atomizers [22].

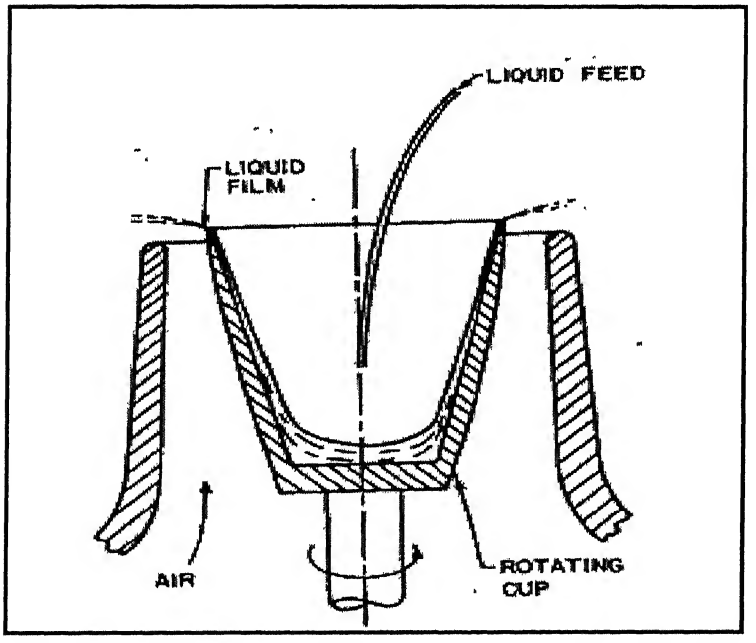


Figure1.2: A schematic of a rotary atomizer [22].

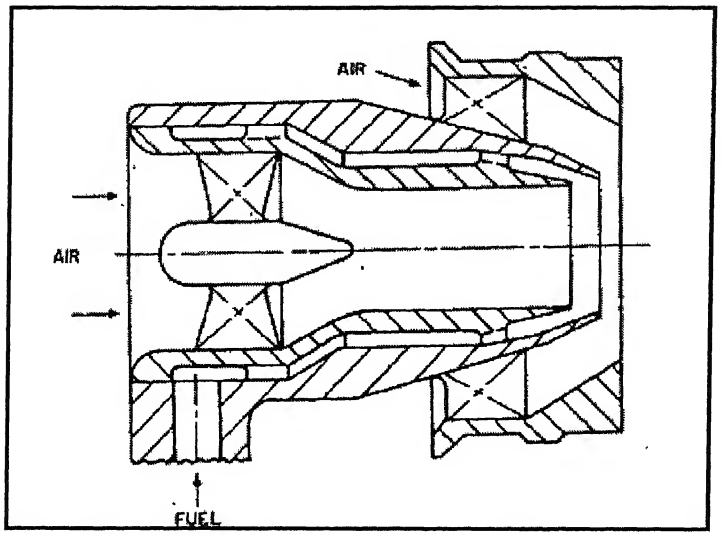


Figure 1.3: A schematic of an air-blast atomizer [22].

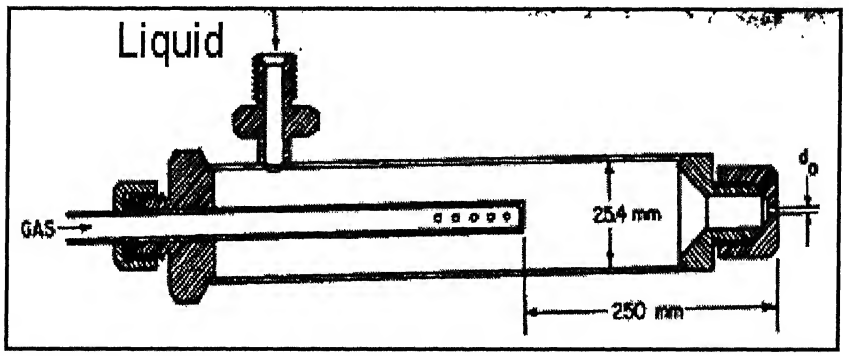


Figure1.4: A schematic of an effervescent atomizer [22].

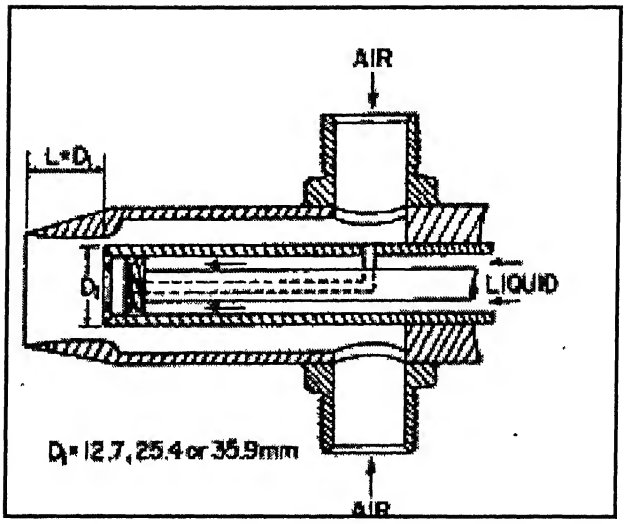


Figure 1.5: A schematic of an internally mixed atomizer [22].

## 1.3 THEORY OF DROPLET FORMATION

The process of atomization is one in which liquid is disintegrated into droplets by the action of internal and /or external forces. In the absence of such forces, surface tension tends to pull the liquid molecules together to form liquid jets or sheets. According to Lefebvre [7], "Atomization can be considered as a disruption of the consolidating influence of surface tension by action of internal and external forces".

The literatures on the theory of droplet formation is quite extensive, but it deals with fairly low velocity and low Reinhold's number flows, which are not very important in practice. Currently, there is no known model of the disintegration of a high velocity liquid discharge. This is due to the highly complex, turbulent and random flow phenomena occurring during disintegration, which is not well understood.

Existing theory of spray formation are based on instability of liquid jets and sheets and are generally based on method of small disturbances [13 – 17]. It is believed that the disintegration of liquid jets or sheets is caused by the waves that form on the surfaces of the jets and sheets of liquid. During instability, these waves rapidly grow into finite amplitude waves that eventually break up the liquid jets or sheets into a multitude of small droplets [18 – 21]. Reitz and Bracco [18] have classified the atomization process into Rayleigh break up; first wind induced, second wind induced and atomization regimes. The Rayleigh regime is governed solely by capillary instabilities, while in the first wind induced regime, the capillary instabilities are enhanced by aerodynamic interaction with the surrounding gas. For the second wind induced and atomization regimes, the break up is characterized by the formation of droplets significantly smaller than jet diameter. It is unfortunate that the atomization regime, which is most important for practical allocations, is the least understood one and no theory that adequately describes the processes occurring in this regime exists [7]. The following table and the corresponding figures describe the atomization processes in a nutshell.

Table A: Classification of jet breakup regimes [7]

| Regime | Description | Predominant drop formation mechanism. |
|---|---|---|
| 1. | Rayleigh breaks up. | Surface tension force, capillary waves. |
| 2. | First wind induced break up. | Surface tension force, dynamic pressure force of ambient air. |
| 3. | Second wind induced break up. | Dynamic pressure of ambient air opposed by surface tension force initially. |
| 4. | Atomization. | Unknown. |

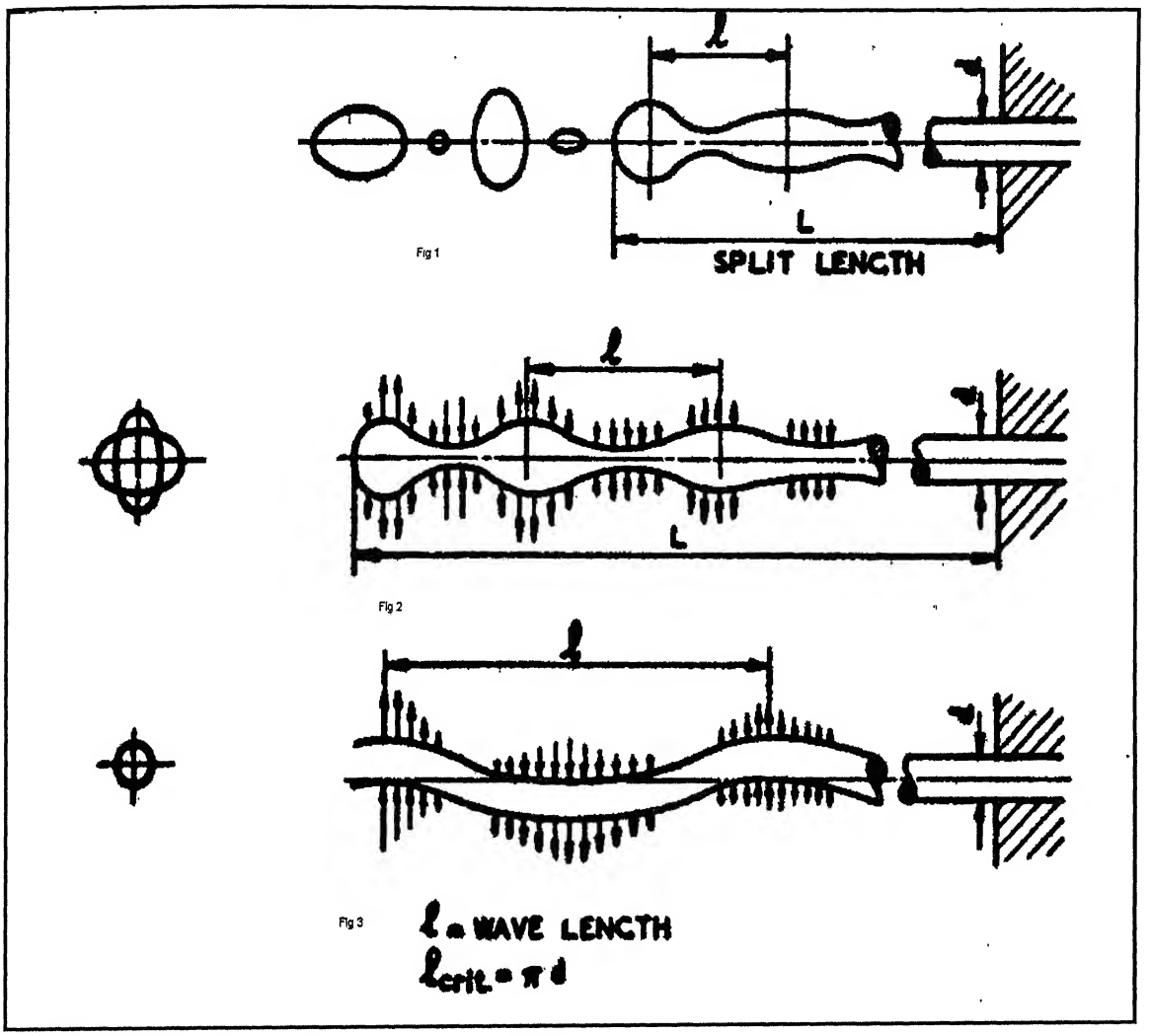


Figure1.6 Liquid jet Disruption [3].

The theoretical basis for the capillary instability was first investigated by Rayleigh [19] who conducted a linear, in viscid analysis neglecting the effects of gas pressure variations on jet distortion. He obtained the following relationship between the initial jet diameter and the droplet diameter.

$$D=1.89\times d.$$

Thus, for the Rayleigh break up mechanism, the average drop size is nearly twice the diameter of undisturbed jet.

Weber [20] developed a linear theory similar to Raleigh's that included the effects of both liquid viscosity and the pressure of the surrounding gas on the jet behavior. He assumed that any disturbance causes rotationally symmetric oscillations of the jet. If the wavelength $\lambda$ of the initial disturbance is less than a particular wavelength $\lambda_{min}$, the surface forces tend to damp out the disturbances. However, if $\lambda$ is greater than $\lambda_{min}$, the surface tension forces tend to increase the disturbances, which eventually leads to disintegration of the jet. There is however, one particular wavelength, $\lambda_{opt}$, that is most favorable for droplet formation, for viscous liquids

$$\lambda_{Min.} = \pi d$$

$$\lambda_{Opt.} = 2^{1/2}\pi d\,[1+ 3\mu_l / (\rho_l \sigma d)^{1/2}]$$

After break up, a cylinder of length $\lambda_{opt.}$ And diameter d forms a spherical drop of diameter D, so that

$$\pi /4\times d^2\times\lambda_{opt.} = \pi/6\times D^3.$$

No simple expression relating droplet size other parameters exist for the wind-induced regime. These fundamentals studies have identified however, an important criterion that governs the formation and break up of droplets. Specifically, the above research points to the existence of a critical value of Weber number, which is the ratio of inertia and surface tension forces acting on the surface of a liquid jet or sheet, above which the liquid flow is very unstable and disintegrates into droplets. The Weber number is defined as

$$W_e=\rho_a V_r D/\sigma$$

Hence, $D = W_e\sigma/\rho_a V_r$

Experimental studies of the disintegration of liquid jet and formation droplets also suggest the existence of a critical Weber number. Griffin and Muraszew [3] suggested that the magnitude of the critical Weber number be between 7 and 12, depending upon flow conditions.

## 1.4 Theory of droplet disintegration

A liquid droplet moving in a gaseous medium will be subjected to certain deformation resulting from the external gas resistance forces ( $R = 3\pi\mu vd$ , for laminar flow $\mathrm{Re} \le 2$, $R = \pi(0.05\rho_a v^2 d^2 + 5\mu vd)$ for semi-turbulent flow $2 \le \mathrm{Re} \le 500$, $R = 0.055\pi\rho_a v^2 d^2$ for turbulent flow $\mathrm{Re} > 500$ ) [2] and the internal forces determined by its surface tension and viscosity. An accurate estimate of the shape and magnitude of such deformations by purely theoretical means is very difficult, mainly because of the lack of information on the pressure distribution around the small moving liquid droplets. As soon as the shape of a droplet changes, the pressure distribution around it will change, and either a state of equilibrium between the external or the internal forces will be reached, or a further deformation will follow, which may ultimately result in the splitting of the droplet.

Different ideas can be found in the literature concerning the causes (mechanisms) of droplet break up by aerodynamics forces. Three of the best grounded hypotheses are

1) Aerodynamics forces exceed the forces of the surface tension which stabilize the inter phase surface
2) Drop deformation exceeds a certain critical value.
3) Unstable oscillations appear (as the drop deforms the frequencies of its induced and natural oscillations become closer to each other, and break up in caused by resonance).

The effect of the variation of air pressure around a droplet was considered by Klusener [3]. If the droplet is in a state of equilibrium, the outer pressure Pa and the surface tension pressure Ps give rise to a pressure Pi inside the droplet, and this internal pressure is constant at any point on the surface.

The surface tension pressure for a surface having radius of curvature $r_1$ & $r_2$ in perpendicular planes is

$$Ps = \gamma(\frac{1}{r_1} + \frac{1}{r_2})$$

And for a sphere this becomes

$$Ps = \frac{2\gamma}{r}$$ Where $\gamma$ = surface tension force (N/m)

The droplet will be stable so long as any change in the air pressure Pa from one point on the surface to another can be balanced by a change in the surface tension pressure such that Pi remains constant . At a point where Pa increases, the droplet will become flatter, thus decreasing the value of Ps, for points where Pa becomes smaller the reverse will occur and a state of equilibrium will be achieved at any instant with a constant value of Pi. If the value of Ps is small enough compared with Pa, then any appreciable change in Pa cannot be balanced by a corresponding change in Ps to keep the value of Pi constant. The outer pressure Pa may then change the shape of the droplet in such a way that a further decrease occurs in Ps at certain points and finally causes the collapse of the droplet, splitting it into two or more smaller droplets. This division immediately increase the value of Ps by reducing the radius r, and Ps may be large enough to accommodate the variations in air pressure Pa. If Ps is still too small, further sub-division will take place until a droplet is obtained so small that its surface tension pressure Ps is large enough to ensure a constant value Pi for all points on the droplet surface.

In general the tendency for the air resistance is to cause distortion and disruption of droplets, and for surface tension and viscosity of the liquid to resist the distortion .Since air resistance varies with the velocity of the droplet relative to the air and also with the density of the air, the variable about which we may speculate are:

1) The injection pressure
2) The properties of the liquid fuel
3) The properties of the surrounding medium

An increase in the discharge velocity diminishes the droplet size. In some experiments droplet size has been found to be inversely proportional to $P^n$ [3]. Where P is the injection pressure and where n is less than unity, and usually less than 0.5.

An increase in either surface tension or the viscosity would cause an increase in droplet size. An increase in density would cause a decrease in droplet size when the around the droplet is turbulent, an increase in viscosity would have similar effect when the flow is laminar.

# CHAPTER II

## Theoretical Study of Helical Passage Pressure- Swirl Atomizer

It is in the atomizer that the pressure energy of the liquid is converted into kinetic energy and applied to the process of disintegration of the liquid jet. The success of the ensuing atomization process will therefore depend greatly on the design and manufacture of the atomizer itself. The swirl-type atomizer differs from the others in that a swirl is imparted intentionally to the liquid while it passes through the atomizer, by means of helical passages incorporated in the atomizer design. This swirling motion under the action of centrifugal force spreads out the liquid in the form of a conical sheet as soon as it leaves the orifice. This sheet then breaks up into liquid droplets under the influence of the external and internal forces. However, the spray produced in this way is usually hollow in the centre and, as compared with the spray from a plain orifice; have larger cone angle, and consequently a lower penetrating power; this makes it more susceptible to any air movement around the spray, and facilitates the mixing process of air and fuel.

These factors, combined with the possibilities of greater simplicity in atomizer design explain the wide interest in swirl atomizers, and it is desirable to consider in more details the nature of the flow in the atomizer, and to attempt to establish a relationship between some of the variables in atomizer design and characteristics of the spray produced.

In this analysis it has been assumed first the flow is non-viscous, and with this assumption formulae have been obtained for the coefficient of discharge and spray angle, expressed as a function of injector dimensions. Then these formulae have been compared with the experimental results in order to see whether they can be modified to allow for the viscosity of the liquid.

### 2.1 Flow in the Atomizer

The liquid enters the settling chamber through helical passage under the action of the injection pressure. The total pressure head is constant through the injector and is equal to that corresponding to the injection pressure head, since it is assumed that liquid is inviscid and no losses occur.

In the swirl chamber the fluid flow is spiral in motion; hence free vortex motion is satisfied.

$v \times r = v_t \times R$; again, $v_t = v_h \cos\beta$,

(Where $v_h$ is resultant velocity through helical passage).

$$\text{So, } v_h = \frac{Q}{nA_H}$$

$$\text{Hence, } v_t = \frac{Q\cos\beta}{nA_H}$$

$A_H$ = cross sectional area of helical passage.

$$\text{Therefore, } v \times r = \frac{QR\cos\beta}{nA_H}$$

At the orifice core radius, we will have;

$$v_2 \times r_a = \frac{QR\cos\beta}{nA_H} \quad ; \qquad \text{(A)}$$

Total head at any point in the fluid is constant and therefore, in the orifice where radial velocity is zero, we can write the Bernoulli's equation;

$$\frac{P}{\rho} + \frac{v_2^2}{2} + \frac{u_2 2}{2} = \text{Constant} = P_S/\rho$$

Where, $P = P_{atm}$

$P_S$ = liquid supply pressure.

For the vortex alone

$$\frac{P}{\rho} + \frac{v^2}{2} = \text{Constant}$$

Hence; $u_2$= constant

$$\text{Therefore, } u_2 = \frac{Q}{A_2 - a_2} \qquad \text{(B)}$$

The value $C_D$ (fictitious coefficient of discharge) is determined by the flowing equation. This fictitious coefficient of discharge takes into account the turning effect of flow.

$$Q = C_D \times A_2 \times \sqrt{2\Delta P / \rho} \qquad \text{(C)}$$

U = resultant velocity in the orifice based on $\Delta P$.

At the core in the orifice where radius is $r_a$, we get

$$\Delta P = \frac{\rho}{2} \times \left( {v_2}^2 + {u_2}^2 \right) \qquad \text{(D)}$$

Where, $\Delta P = P_S - P$

Putting the values of $v_2$ and $u_2$ in equation (D) and using equation (C) we get

$$\frac{1}{{C_D}^2} = \frac{{A_S}^2}{(1-\phi)} + \frac{1}{\phi^2}; \qquad \text{(E)}$$

where, $\phi = \dfrac{A_2 - a_2}{A_2}$

where, $A_S = \dfrac{\Pi R r_2 \cos\beta}{n A_H}$

For maximum discharge the value of $C_D$ should be made maximum i.e. the air core should be such that it will give maximum discharge.

Differentiating the above equation with respect to $\phi$; we get

$$A_S = \frac{(1-\phi) \times \sqrt{2}}{(\phi)^{3/2}} \qquad \text{(F)}$$

Since, the value of $\phi$ is a function of $A_S$, it is evident that the fictitious co-efficient of discharge is, theoretically, a function of only of this atomizer constant, and is independent of liquid supply pressure when the air-core is fully developed.

Therefore, $$C_D^2 = \frac{1}{\dfrac{1}{\phi^2} + \dfrac{A_S^2}{(1-\phi)}} \qquad \text{(G)}$$

2.1.1 For Spray cone angle (scattering)

Mass flow per unit time through the orifice = $2\pi r\rho u_2 dr$

[$u_2$ = Constant through orifice proved previous]

Tangential velocity in the Orifice

$$v = \frac{QR\cos\beta}{nA_H} \quad \text{(obtained previously) (H)}$$

Hence, momentum in the tangential flow for elementary ring in the orifice

$$= \frac{2\pi\rho u_2 QR\cos\beta dr}{nA_H} \qquad \text{(I)}$$

Total momentum in the tangential flow in the orifice

$$= \frac{2\pi\rho u_2 QR\cos\beta(r_2 - r_a)}{nA_H} \qquad \text{(J)}$$

Again total mass flow through orifice = $\rho u_2(A_2 - a_2)$

Mean tangential velocity

$$\bar{v} = \frac{2\pi(\rho u_2)QR\cos\beta(r_2 - r_a)}{(A_2 - a_2)nA_H(\rho u_2)} \qquad \text{(K)}$$

$$= \frac{2\pi QR\cos\beta(r_2 - r_a)}{(A_2 - a_2)nA_H}$$

$$u_2 = \frac{Q}{(A_2 - a_2)}$$

Therefore,

$$\tan\alpha = \frac{\bar{v}}{u_2} = \frac{2\pi QR\cos\beta(r_2 - r_a)}{nA_H} \qquad \text{(L)}$$

$$= \frac{2\pi R r_2 \cos\beta\left(1-\frac{r_a}{r_2}\right)}{nA_H}$$

Now, $\phi = \frac{A_2 - a_2}{A_2} = 1 - \left(\frac{r_a}{r_2}\right)^2$

$$\frac{r_a}{r_2} = \sqrt{1-\phi} \qquad \text{(M)}$$

$$\tan\alpha = \frac{2\pi R r_2 \cos\beta\left(1-\sqrt{1-\phi}\right)}{nA_H}$$

$$= \frac{2A_S\left(1-\sqrt{1-\phi}\right)}{1} \qquad \text{(N)}$$

Where, $A_S = \frac{\pi R r_2 \cos\beta}{nA_H}$

Again $A_s = \frac{\sqrt{2}(1-\phi)}{\phi^{3/2}}$

so, putting the value of $A_S$,

$$\tan\bar{\alpha} = \frac{2x\sqrt{2}(1-\phi)}{\phi^{3/2}} x\left(1-\sqrt{1-\phi}\right)$$

By manipulating, $\bar{\alpha} = \tan^{-1}\frac{\sqrt{8}(1-\phi)}{\left(1+\sqrt{1-\phi}\right)\sqrt{\phi}}$

The calculated value of the cone angle would not be constant across the issuing jet, because the values of the tangential and axial velocity components at exit vary with the value of **r**. The tangential velocity decreases with increasing radius, from the air core outwards and the axial velocity increases with increasing radius. Hence **tanα,** given by **(v/u)**, will be greatest at the air core and least at the outside surfaces of the issuing jet Therefore, the streams of liquid at the inner and outer surfaces of the issuing jet will tend

to penetrate one another, and will generate intense turbulent in the thinning layer of liquid, thus tending to promote early disintegration and good atomization of spray

The theoretically estimated variations in $C_D$, $\alpha$ and $\phi$ with respect to $A_S$ are shown in figures [2.1, 2.2, 2.3] and are discussed in detail at the end of the atomizer design in chapter III.

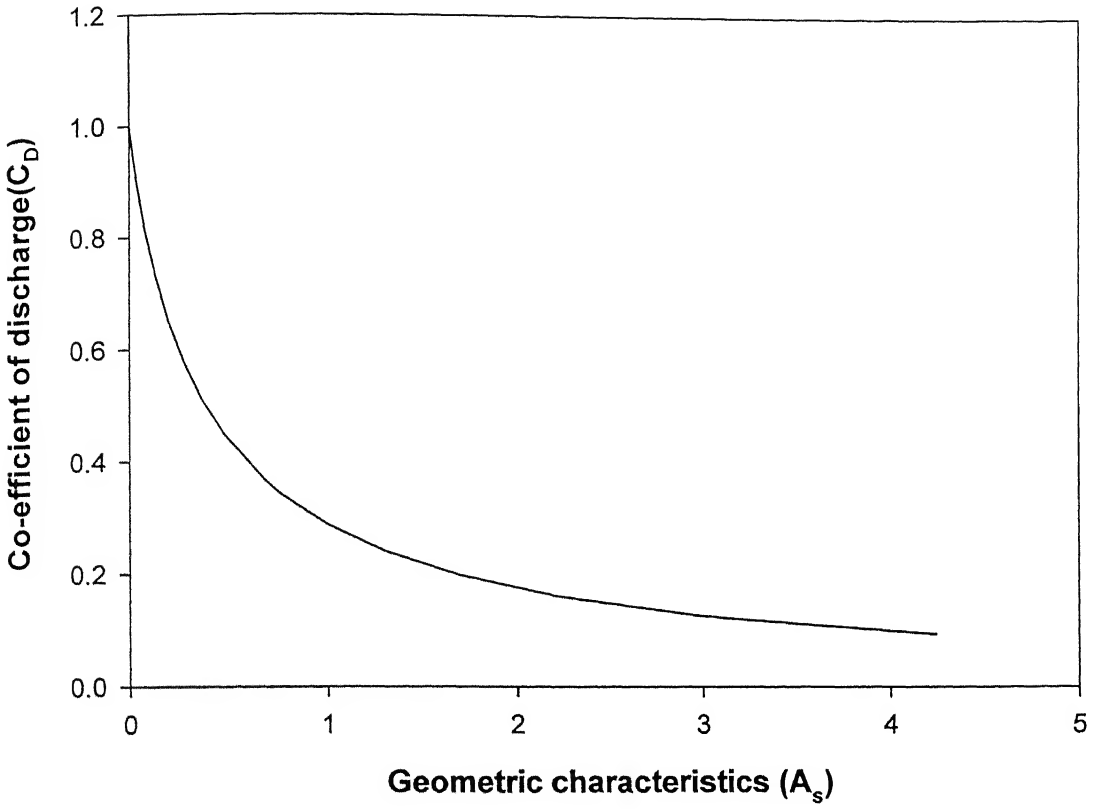


Figure 2.1 Dependence of $C_D$ with non-dimensional geometric characteristic.

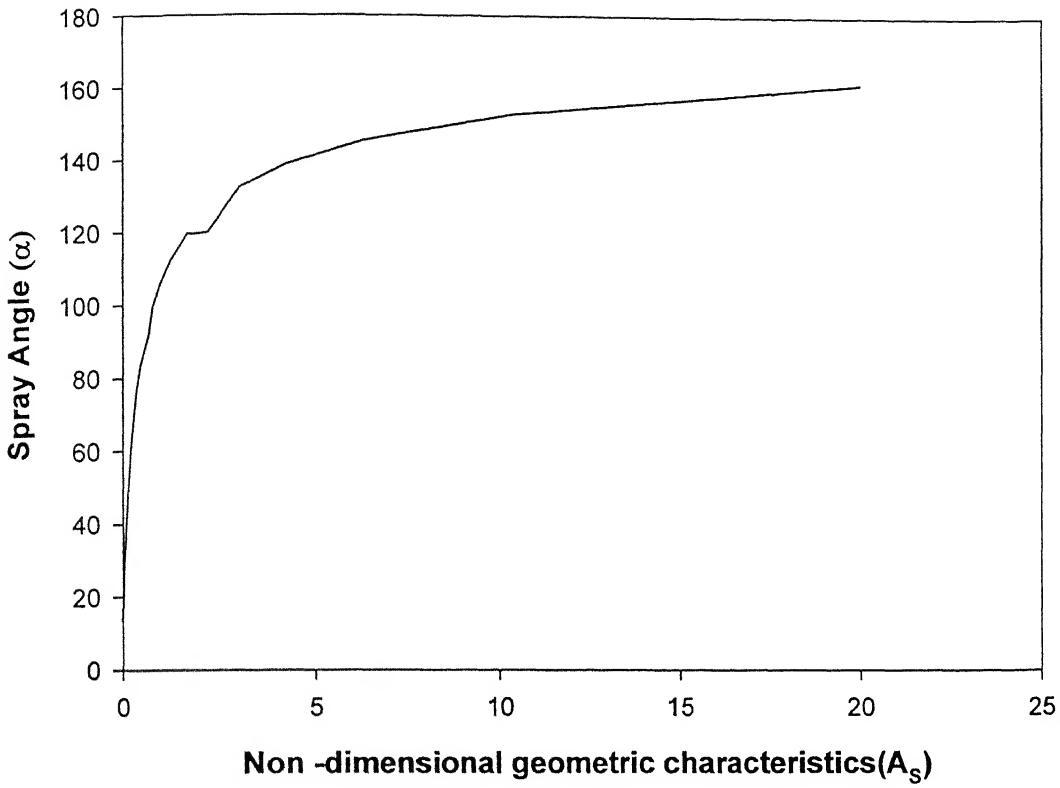


Figure 2.2 Dependence of α with non-dimensional geometric characteristics ($A_S$).

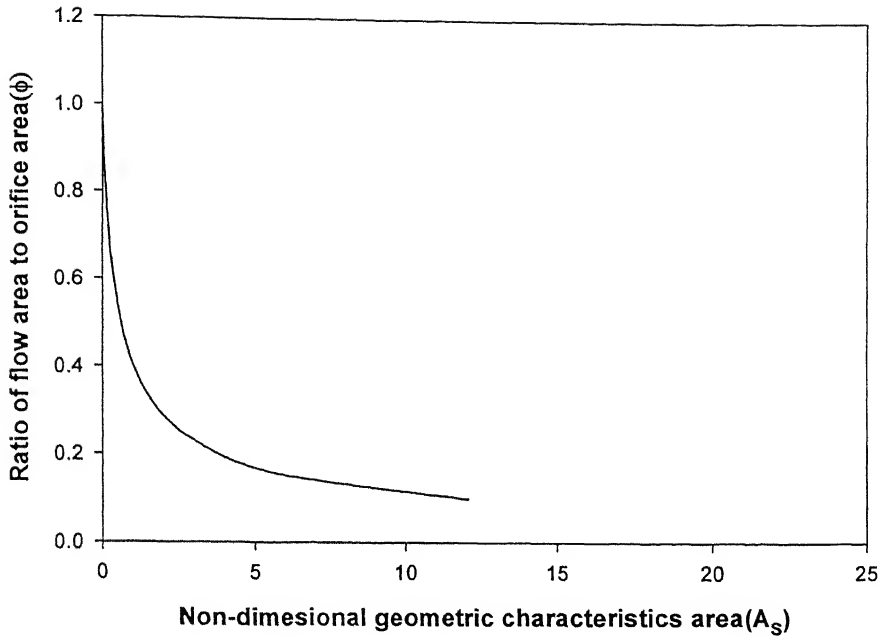


Figure 2.3 Dependence of $\phi$ with non-dimensional geometric characteristics ($A_S$). .

## 2.2 Air Core

The shape and size of the air core in a pressure swirl atomizer have been studied by different investigators [11], by means of an atomizer made from transparent material. The observations have shown that both the shape and the air core and its size are not in agreement with theoretical predictions which neglect the viscosity of the liquid.

Theoretically the relative size of the air core in the settling chamber, spin chamber and in the orifice can be deduced from the equation for the total heat in the liquid. This gives $v^2 + u^2 =$ constant, at the air core. Since, u is greater in the orifice, a smaller value of v implies a larger diameter of air core, and therefore, the air core in the orifice is larger than in the spin chamber and the settling chamber. Also, since the axial velocity is constant along the length of the orifice, so also the tangential velocity. The shape of the air core is therefore, cylindrical in the orifice. Similarly, for the same reason the air core will be conical in shape in the spin chamber and cylindrical in the settling chamber, but of reduced radius.

Progressive air core development has been shown in the following figures:

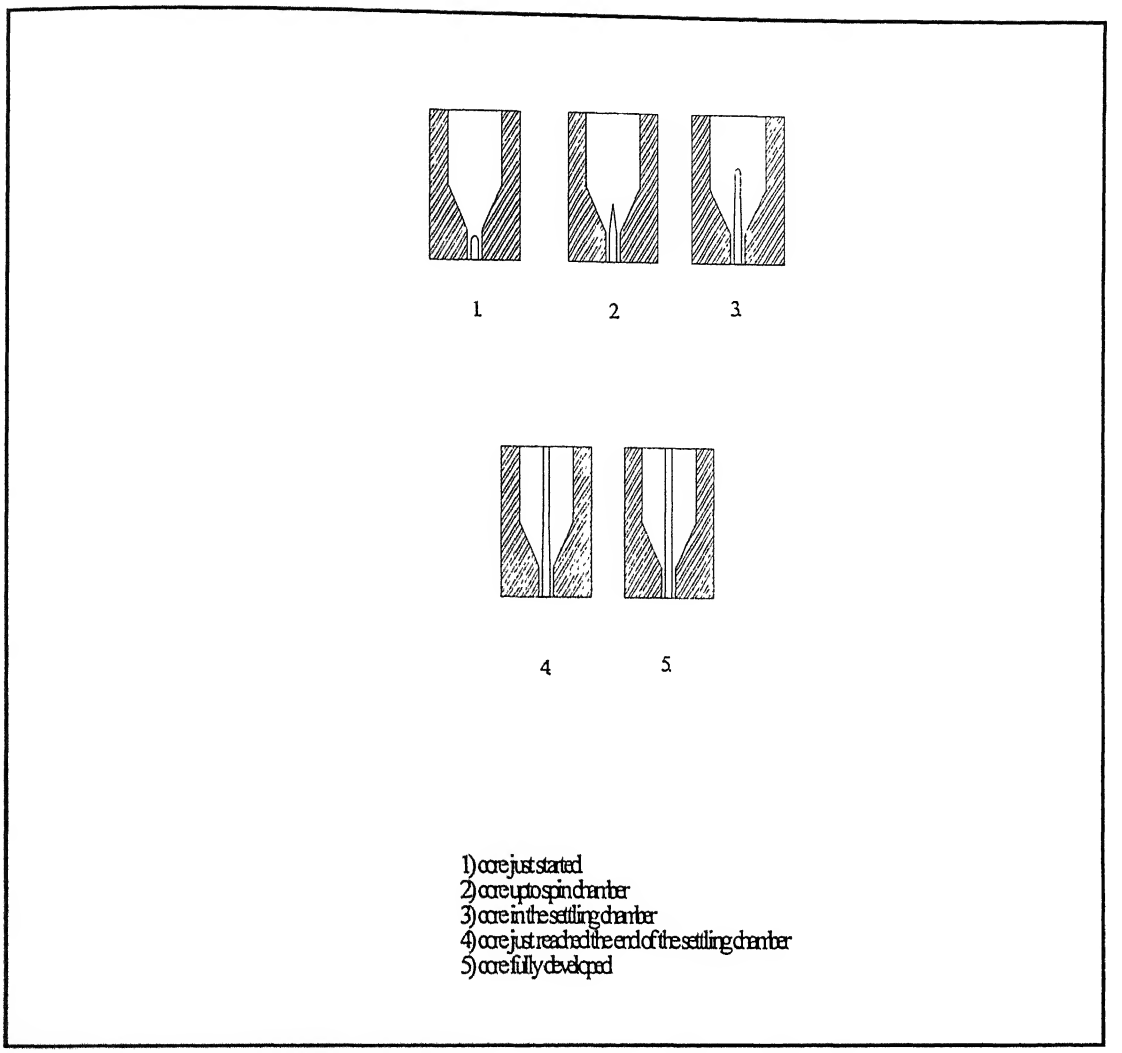


Figure 2.4 Development of air core in pressure-swirl Atomizer.

# CHAPTER III

## ATOMIZER DESIGN

There are two factors to the design of atomizer flow geometry. The first involves the determination of the combustion field, which is acceptable in terms performance, stability, and hardware durability. The second is a specific design of a flow system geometry, which will produce the desired combustion field. Normally, flow system geometry is design based on some selected geometrical and flow parameters, and the resulting combustion is calculated, since working backward from a combustion field to an injector flow system geometry is extremely difficult and does not result in a unique geometry .thc actual flow geometry is composed of three parts:

1) The total element pattern
2) The individual orifice geometry
3) The geometry of the flow system upstream of the orifice.

**3.1 Design Procedure**:-

(A) Specific parameters:

Total volume flow rate m =0.05-0.25$m^3/s$

Density $\rho = 1000 Kg/m^3$

Viscosity $\mu = 0.001$ N.s/$m^2$

Surface tension $\sigma = 0.0735$ N/m

(B)Expected parameters:

Pressure drop: $\Delta p = 0.28\text{-}8.5$ bar

Length: L= 45mm

(C) Calculation of basic parameters and dimensions of Helical – cum- pressure-swirl atomizer for water.

Assuming ideal fluid behavior, the geometric characteristics of the helical atomizer is described by:-

$$A_S = \frac{\pi R r_2}{n A_H} \cos\beta \qquad (1)$$

where R=average (mean) radius of helical passage

$r_2$=orifice radius

N= number of turns of the helical passage

$A_H$= helical passage cross-section area

β= angle between helical passage axis and tangential direction perpendicular to the atomizer axis.

$A_S$ = geometric characteristics of the injector

$A_S$ = 1.57 (taken)

Number of turns of the helical passage N, may be selected in order to obtain desired value of $A_S$ and helical passage length. The value of N may be taken in the range of 1 to 8.

N=2 (taken)

Number of helical ports n may be provided in the range of 2 to 4 to provide uniform distribution of water stream in the settling chamber with two ports,

n =number of helical ports

= 2 (taken)

The non-dimensional velocity $V_R$ at the outlet of the helical passage is given by

$$V_R = \frac{axialvelocity}{\tan gentialvelocity} = \frac{Va}{Vt} = \tan\beta \qquad (2)$$

Where β is the angle made by the water stream in the helical passage with the horizontal. The value of $V_R$ may be taken in the range of 0.24 to .04.

$V_R$= 0.256 ( taken), and β= $14.263^0$ (taken)

The orifice diameter $d_2$ of the element can be obtained from relation:

$$d_2 = \left[\frac{4m}{\pi C_D \sqrt{2\rho 4p}}\right]^{1/2} \quad (3)$$

$C_D$= Fictitious co-efficient of discharge.

= 0.28 (taken from plot, figure 2.1)

$$d_1 = 2.4\, d_2 \quad (4)$$

where, $d_1$= outer diameter of screwed element.

$\tau$ = pitch of the helical; path

$$= \pi d_1 \tan\beta \quad (5)$$

Axial length of the helical passage

$$L_2 = 4\tau \quad (6)$$

$L_H$ = overall length of the helical passage

$$= \frac{nL_2}{\sin\beta} \quad (7)$$

Trapezoidal cross-section of the helical passage is considered to be more suitable from manufacturing point of view. So a trapezoidal cross section is selected.

Width of the trapezoidal section at the outer periphery b is calculated from:

$$b = \frac{\tau - 1}{2} \quad (8)$$

Mean radius of the helical passage, $(R) = d_1/2 - b/2 \cos\beta$ (9)

$$A_H = \frac{\pi R r_2}{nAs}\cos\beta \quad (10)$$

Where, $A_H$ = area of the helical passage.

Depth of the helical passage, $(h) = \frac{d_1 - c}{2}$ (11)

c= 0.3 mm = a constant

Inner width of the section is given by

$$a = \frac{2A_H}{h} - b$$

$$v_h = \frac{m}{\rho n A_H} \tag{12}$$

$$v_t = \frac{v_h}{\sqrt{1+\tan^2\beta}} \tag{13}$$

$\mathrm{Re}_t = \frac{\rho V_t d_1}{\mu}$ = Reynolds's number at the inlet.

Now, for fully developed gas core

$$As = \frac{\sqrt{2}(1-\phi)}{\phi^{3/2}} \tag{14}$$

Where $\phi$ = orifice area co-efficient by solving

$$\phi = 1 - \left(\frac{2ra}{d_2}\right)^2 \tag{15}$$

$r_a$ = Gas core radius

$$C_D = \frac{1}{\left[\frac{1}{\phi^2} + \frac{As^2}{(1-\phi)}\right]^{1/2}} \tag{16}$$

$L_2 = 4\tau$

$L_3 = 0.5\ d_1$

$L_3$ = settling chamber length.

$$L_4 = \frac{d_1 - d_2}{2} \cot\theta$$

$L_4$ = spin chamber axial length.

$\theta = 23^0$ (semi convergence angle of the spin chamber)

$$L_1 = L-(L_2+L_3+L_4+L_5)$$

where, $L_5 = 2.0$ mm (orifice length).

(D) Determination of pressure losses:

(1) Entrance section (A):

Flow velocity at the inlet section:

$$V_A = \frac{m}{\rho A_1} \qquad (17)$$

$$R_{eA} = \frac{\rho d_1 v_A}{\mu}$$

Since $R_{eA} > R_{eA\ critical} = 2300$

The flow is turbulent in the inlet section.

Friction factor can be calculated as –

$$\frac{1}{\sqrt{4f_a}} = 2\log\left(R_{eA}\sqrt{4f_A}\right) - 0.8 \qquad (18)$$

$$\Delta P_A = f_A x \frac{L_1 \rho V_A^{\ 2}}{2d_1} \qquad (19)$$

(2) pressure drop in helical passage :-

$$d_H = \sqrt{\frac{4A_H}{\pi}} = \sqrt{\frac{2Rd_2 \cos\beta}{nA_S}} \qquad (20)$$

$d_H$ = equivalent diameter of helical passage.

$$R_{eh} = \frac{\rho d_H V_H}{\mu}$$

$$R_{eHcrit} = 2\left(\frac{d_H}{d_t}\right)^{0.32} x10^4$$

Since, $R_{eH} > R_{eHcrit.}$

Friction factor for straight injector is given by –

$$f_{st} = \frac{0.316}{R_{eH}^{1/4}}$$

$$f_H = f_{st}\left[R_{eH}\left(\frac{d_H}{d_1}\right)^2\right]^{1/20} \qquad (21)$$

$$\Delta P_H = f_H x \frac{L_H \rho V H^2}{2d_H}$$

(3) pressure drop in the orifice section

$$\Delta P_W = \frac{m^2}{2C_D{}^2 A_2{}^2 x\rho} \qquad (22)$$

And $A_2 = \frac{\pi d_2{}^2}{4}$

$\Delta P=\Delta P_A+\Delta P_H+\Delta P_W$ = total drop in pressure in the element due to friction.

((E) Mean spray angle :-

$$\tan\alpha = \frac{\sqrt{8}(1-\phi)}{\left(1+\sqrt{1-\phi}\right)x\sqrt{\phi}} \qquad (23)$$

(F) Calculation of thickness :-

$P_i$= Driving pressure required

$(P_{atm.} + \Delta P)$ bar

Considering factor of safety =1.5

$$t = 1.5r_i\left[\left(\sqrt{\frac{2\tau_s}{\tau_s - 2p_i}}\right) - 1\right] \qquad (24)$$

$\tau_s$ = Shear strength of brass

(G) diameter of the screws for fluid tight joint

$$d_s = 2840\ p_i \qquad (25)$$

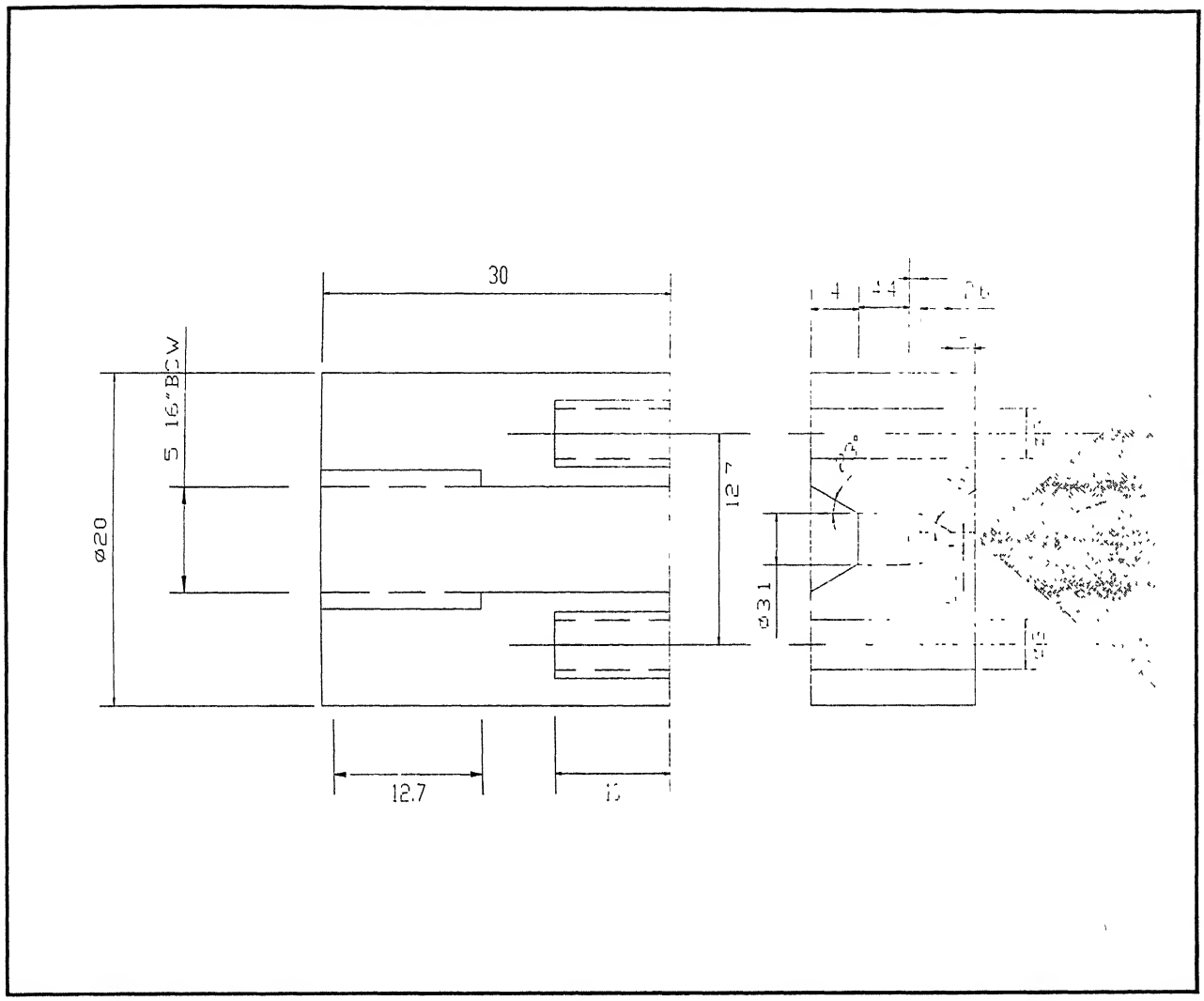


Figure3.1 Schematic diagram of Injector designed.

## 3.2 Effect of various parameters on the performance of atomizer

1) Effect of helix angle (β):- At the given operating condition an increase in helix angle will cause an increase in area co-efficient, co-efficient of discharge and spray penetration, but it will cause decrease in spray angle and bigger droplet size. Because as helix angle is increased swirl is reduced, hence less tangential velocity $\left( V_t = \frac{V_R}{\sqrt{1+\tan^2 \alpha}} \right)$. As tangential velocity takes active part in disintegrating the liquid sheet and controls the spray angle, helix angle is an important parameter to be looked into. Because of reduced spray angle cooperation of air force in disintegrating the jet is also reduced. The increase in co-efficient of discharge is due to more energy appearing in axial direction. Co-efficient of area $\phi$ (measure of droplet size) will increase because of reduced tangential velocity, so helix angle should be chosen with utmost care in order to have desire spray cone angle, droplet size, penetration, distribution & dispersion.

2) Effect of number of port (n):- increase in number of ports gives rise to uniformity to the flow, hence less losses causing higher Cd and $\phi$ , but lower spray cone angle.

3) Effect of number of turns (N): - It gives rise stability to the flow in the helical passage, but as number of turn increases, fluid friction loss as well as secondary flow loss increases and decreases co efficient of discharge.

4) Effect of mean radius of the helical passage (R):- As R decreases; it gives rise to uniformity to the flow. As radius increases, non-uniformity to the flow increases causing more losses in the atomizer and reduces Cd and $\phi$ but increases $\alpha$ .

5) Effect & spin chamber: - It is provided to make the flow more uniform in the orifice and to avoid formation of vena-contracta. We have seen in pipe flow that sudden contraction results eddies losses with consequent decrease in co-efficient of discharge.

6) Effect of settling chamber: It is provided to damp out unwanted turbulence in the flow issuing from helical passages. Apart from that settling chamber minimizes the impact loss arising from the spin chamber.

7) Effect of orifice diameter ($d_2$):- Pressure-swirl atomizer is very sensitive to orifice diameter .Everything remaining constant, an increase in orifice diameter will decrease the axial velocity at the outlet of orifice but tangential velocity will substantially remain constant, or even may increase. The result is that the co-efficient of discharge as well as penetration will decrease. Because more energy will appear in the tangential direction.

8) Effect of orifice length (L):- This length involves losses in the atomizer. As the value of $C_d$ takes care of losses, $C_d$ will decrease first, then increases reaching an optimum value it will start decreasing. This is explained with respect to the position of vena-contracta. When there is no re-attachment of flow, loss will increase. When re-attachment occurs within the orifice, loss will decrease, hence consequent increase in $C_d$. This is because the space around the vena-contracta will decrease, hence eddies losses. Further increase in length will result friction loss, hence $C_d$ will decrease again.

9) Effect of surface finish: - Surface finish promotes laminar flow or turbulent flow depending upon whether the surface is smooth or rough. Rough surface promotes turbulence. Since velocity & pressure at a particular point in the atomizer are not constant with respect to time, depending upon situation turbulence may give rise to increased energy oscillation or may be damped out. Energy oscillations or waves because of turbulence interacting with the external air force result in break up of jet. However, whatever may be the case, in pressure-swirl atomizer tangential velocity & turbulence overcome the surface tension force of the liquid to form droplet at lower air density.

# CHAPTER IV

## Experimental study of helical passage swirl type atomizer

This chapter describes the experimental investigation of the performance of a helical passage swirl type atomizer. It describes the experimental set up developed to study the dependence of injector's performance upon various operating condition, e.g., liquid flow rate, liquid supply pressure. This chapter also describes the mode in which the injector must be operated to obtain almost same spray cone angle or to obtain different droplet sizes.

A cross-sectional view of the helical passage swirl type injector tested in this study is shown in Fig.3.1. Liquid enters through the threaded opening of a tube of 1.5 mm radius that extends up to spin chamber shown in Fig. 3.1. Between the spin chamber and entrance section, a screwed element is pressed fit, leaving a settling chamber between the end of screwed element and the spin chamber. Double threaded screwed element has been used, Acme thread of cross sectional 0.455 $mm^2$. The spin chamber is of conical shape of $46^0$ in order to avoid the formation of vena-contracta in the orifice which is of 0.8 mm in diameter.

To facilitate manufacturing, we have used brass because of its softness, ductility and excellent machinability.

4.2 Design of Test Rig:

The main components of the test rig are:

1. pressurized water container
2. pressure regulating valve (0-9 bar)
3. gate valves (3)
   a) For supplying air pressure to water container placed at the top
   b) Supplying pressurized water to injector entrance
   c) Relieving air pressure at the end of the experiment placed at the top of the container
4. Passage nuts (2)
   a) For supplying water at the top of pressurized container

b) For removing sludge at the bottom of the pressurized container

5. Filter
6. Rotameter
7. Copper tubes
8. Pressure transducer
9. Water reservoir
10. Stand for rotameter
11. CCD camera
12. Lenses
13 LASER
14. P.C

Entire set up is shown in the Fig.4.3.

In experiment, we have tried to use standard elements readily available in the market. How ever some of the elements are purchased from the market and some were readily available in our lab.

4.2.1 Design of pressurized container:-

The material we have used is cast iron hollow cylinder. The cast iron is brittle material and, hence maximum principle stress theory will hold good. According to this theory the thickness is related to pressure and tensile strength.

$$t = r_i x\left(\sqrt{\frac{\sigma_t + p}{\sigma_t - p}} - 1\right)$$

$r_i$=internal radius

$\sigma_t$ =tensile strength

p= pressure

During experiment our cylinder pressure $p << \sigma_t$. So no chances are for failure and our existing cylinder thickness $t >> t_{th}$. This will enable us to conduct experiment in future at higher pressure.

4.2.2 Thickness of the tube:-

$$t = \frac{P_i D_o}{2\sigma_t} \qquad D_o = \text{Out-side Diameter.}$$

Where p= 0-9.0 bar

For this pressure, the copper tube thickness is smaller than the used one. Hence, there is no problem of bursting.

4.2.3. Rotameter:-

The Rotameter was purchased and was calibrated for aviation turbine fuel of specific density 0.8. So for our purpose we needed to calibrate it again. Calibration is done to get the correction factor for water and a plot was made flow rate ($m^3/s$) vs. Rotameter scale.

Theoretical correction factor

$$K_{th} = \sqrt{\frac{\rho_{ATF}}{\rho_{WATER}}} = \sqrt{0.8} = 0.89$$

So, water flow rate (m3/s)

$$Q_{WATER} = K_{th} \text{ X Rotameter scale}$$

## 4.3 Rotameter Calibration procedures

The calibration set up is shown schematically in Fig.4.1. High pressure air is introduced into a cast iron vessel to drive water through a filter and Rotameter to a measuring jar. An electronic balance is used to measure weights of the water collected in the jar for 30 seconds at different flow rate and corresponding scale readings were taken from the rotameter scale. Then the scale reading was converted to volume flow rate in liter/min. and corresponding experimental correction factors were calculated. Average value of the correction factors gives overall picture of the Rotameter.

$$(k_{exp}) = \frac{volumeflowrateofwater(lit/\min)}{correspondingreadingofrotameterscale}$$

$K_{Average} = (K_1+K_2+K_3+ \text{----------}+K_N)/N$

The experimental average calibration factor was estimated to be equal to 0.891 which is exactly equal to 0.89 estimated theoretically.

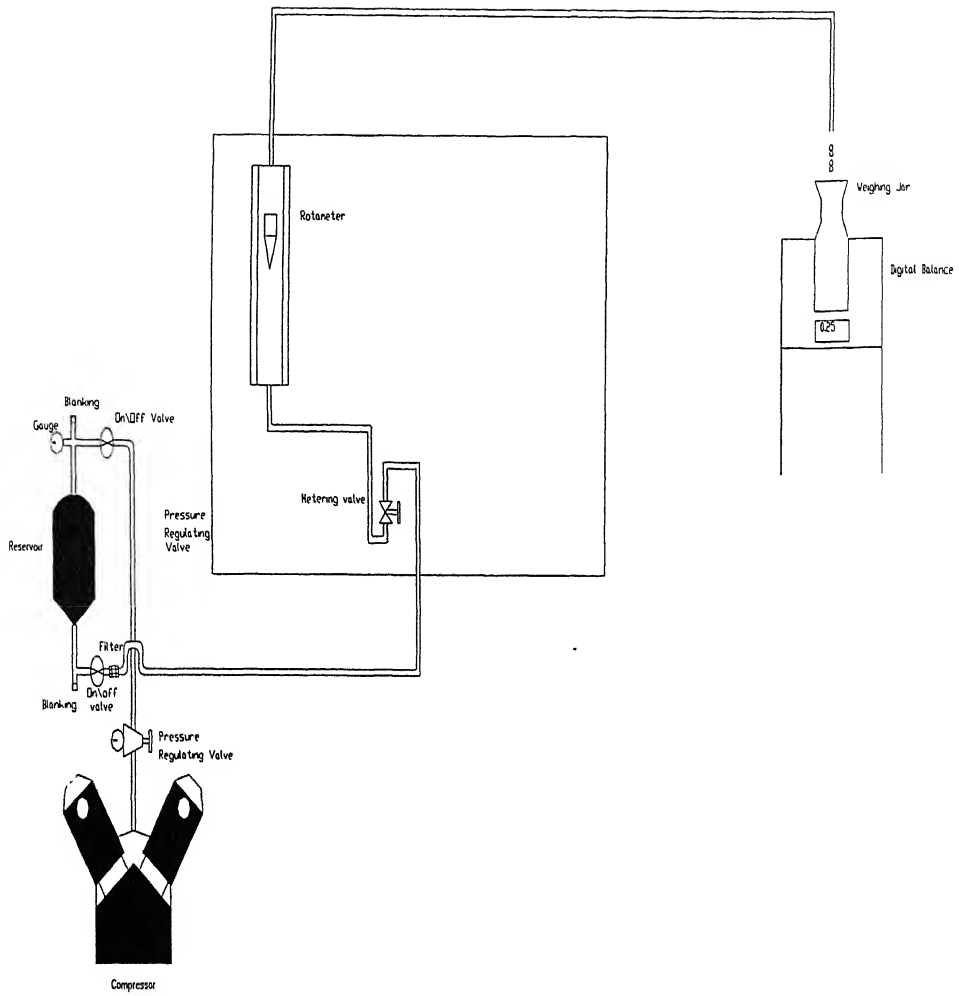


Figure 4.1 Schematic diagrams for rotameter calibration.

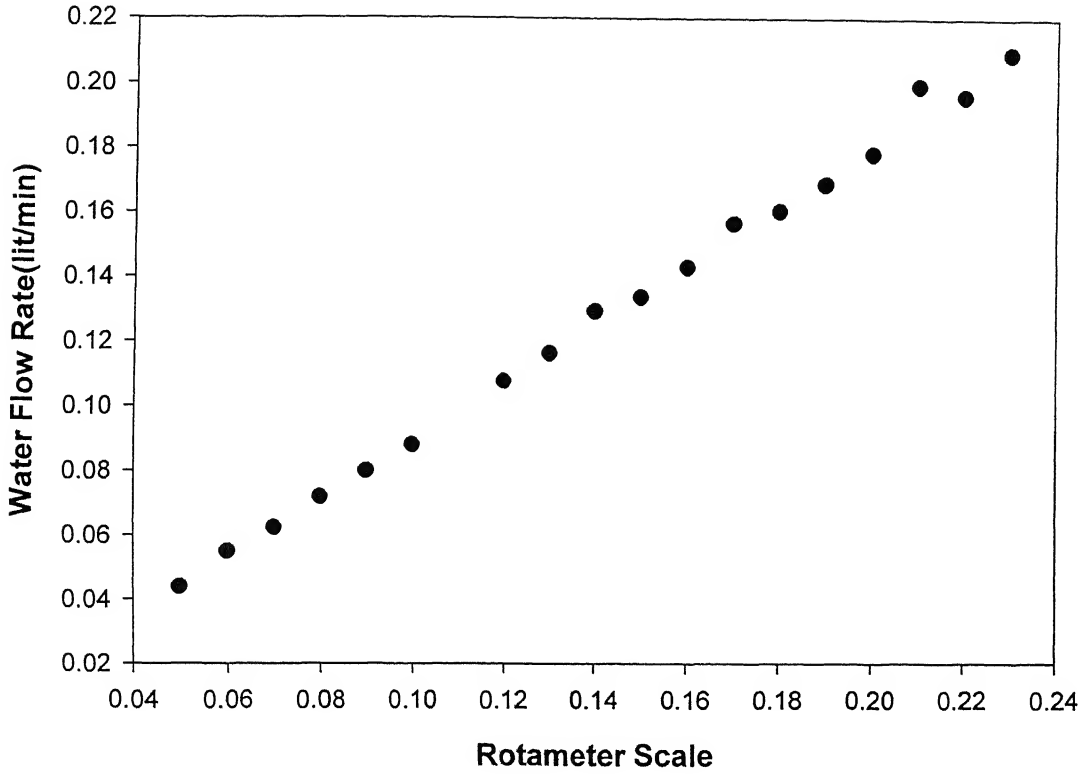


Figure 4.2: Water flow rate (lit/min.) vs. Rotameter scale reading.

## 4.3 Experimental procedure

The experimental set up is shown schematically in figure 4.3. High pressure air is introduced into a cast iron pressure vessel to drive water through a valve, filter, metering valve, flow meter and then through the helical passage pressure –swirl atomizer. A pressure transducer is used to measure the fluid injection pressure $\Delta p$. The injection pressure was varied from 0.28 bars to 8.53 bars by adjusting the metering valve. The orifice diameter $d_2$ is 0.8 mm and the minimum and maximum flow rate are 0.0445 litre/min. and 0.2189 litre/min. respectively. At the maximum flow rate, average spray forms $80^0$ cone angle.

The atomization process from a hollow –cone spray and is investigated by CCD camera connected to computer terminal. First a LASER sheet was made by using a cylindrical lens. The laser sheet is passed through centre line of the hollow cone. Perpendicular to LASER sheet CCD camera was focused and the images were captured in the computer. Suitable exposure time was maintained to see the break length and movies were taken at different flow rates. At different flow movies are analyzed and average break-up lengths were calculated.

The detail of the experimental setup is shown in Fig. 4.3

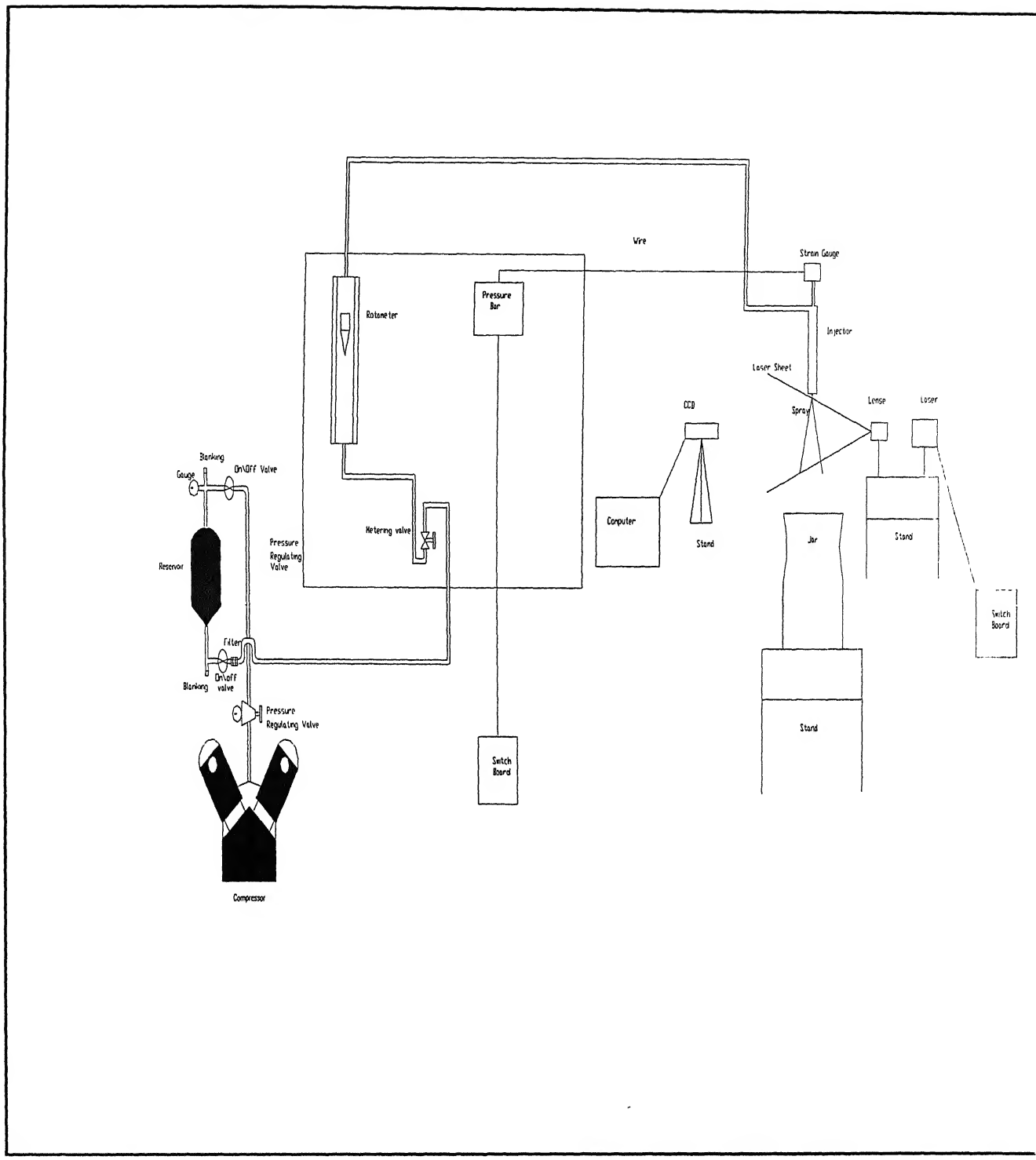


Figure 4.3 Schematic diagram of experimental setup.

# CHAPTER V

## Results and discussion

### 5.1 Experimental effort

In order to identify various parameters that affect the performance of helical passage pressure –swirl atomizer, an experimental study of the injector was carried out. The experimental investigation included studies of the effects of the liquid supply pressure, Reynolds number ($R_e = \rho U d_2/\mu$) which is the ratio of inherent force to viscous force, and gas Weber number ($W_e = \rho_a U^2 d_2/\gamma$) which is the ratio of inertia force to surface tension force on the performance parameters of the injector. The effect of Froud number, the ratio of inertia force to gravity force has not been studied because of its negligible effect on the performance of atomization process. The liquid supply pressure and flow rate were measured and their dependence upon the flow parameters and performance parameters were studied. The measured data were then analyzed to gain insight into the physics of the atomization process.

### 5.2 Effect of supply pressure

The liquid pressure plays the most significant role in the atomization process in pressure swirl atomizer. Varying the supply pressure of liquid changes the tangential velocity (responsible for jet break up & atomization) an axial velocity (causing flow through the orifice) and, thus, the magnitude of the air forces acting on the liquid sheet. This, in turn changes the spray cone angle (may vary little if core is fully developed) and the size of the droplet produced by the injector. The effect of the pressure on the performance of the injector was studied by changing the pressure upstream of the injector which is positioned vertically downward in the atmosphere. The supply pressure is increased gradually from .28 bars to 8.53 bars by opening the needle valve installed upstream of the Rotameter (to measure corresponding flow rate). From the Rotameter scale flow rate is measured and multiplied by correction fáctor to water flow rate. Series of photographs at different $\Delta P$ is shown in figure 5.1 (a - r) Resultant velocity (U) at the injector is calculated based on pressure difference $\Delta P$. The results plotted in figure 5.2 and 5.3 describe the dependence of velocity and Reynolds number on liquid supply pressure.

## Evolution of spray in pressure-swirl atomizer

Figure 5.1 (a) and (b)

From pressure 0.41 bars to 0.58 bars, the magnitude of tangential velocity (magnitude of inertia force in tangential direction) is not sufficient enough to open the bulb. Hence, the issuing jet is cylindrical in shape. Break up of jet is caused by rotationally symmetric oscillations with additional effect of air force.

Figure 5.1 (c)

Formation of nuclei of bulb due to higher tangential velocity, as pressure is increased from 0.58 bars to 0.88 bars. The nuclei of bulb is seen to be dancing just at the exit of the atomizer. The dancing of the bulb is caused by inherent instabilities of the turbulent flow in the atomizer.

Figure 5.1 (d), (e), (f), (g), (h), (i) and (j)

Growth and development of the nuclei of the bulb. At this stage from pressure 0.88 bars to 3.44 bars, though inertia forces in the tangential direction increases, it is still not strong enough to overcome the consolidating influence of increasing surface tension force. But at this stage the sheet is thinned down and any disturbances of higher magnitude can cause it to disrupt. However, at this pressure range break up is caused by mutual impingement of the converging sheet (because of surface tension and decreasing inertia force) and by higher magnitude air friction with waviness of the sheet.

Figure 5.1 (k)

This shows the opening of the bulb and implies the fully developed air core. At this pressure (34.4 bars) inertia force is strong enough to surmount the consolidating influence of surface tension force and the bulb is opened. Formation of ligaments and non-uniform droplet is seen at the end of sheet break up length.

Figure 5.1 (l) and onwards:

Break up length decreases, because at higher pressure greater than 3.44 bar the required inertia force to disrupt the sheet is reached earlier.

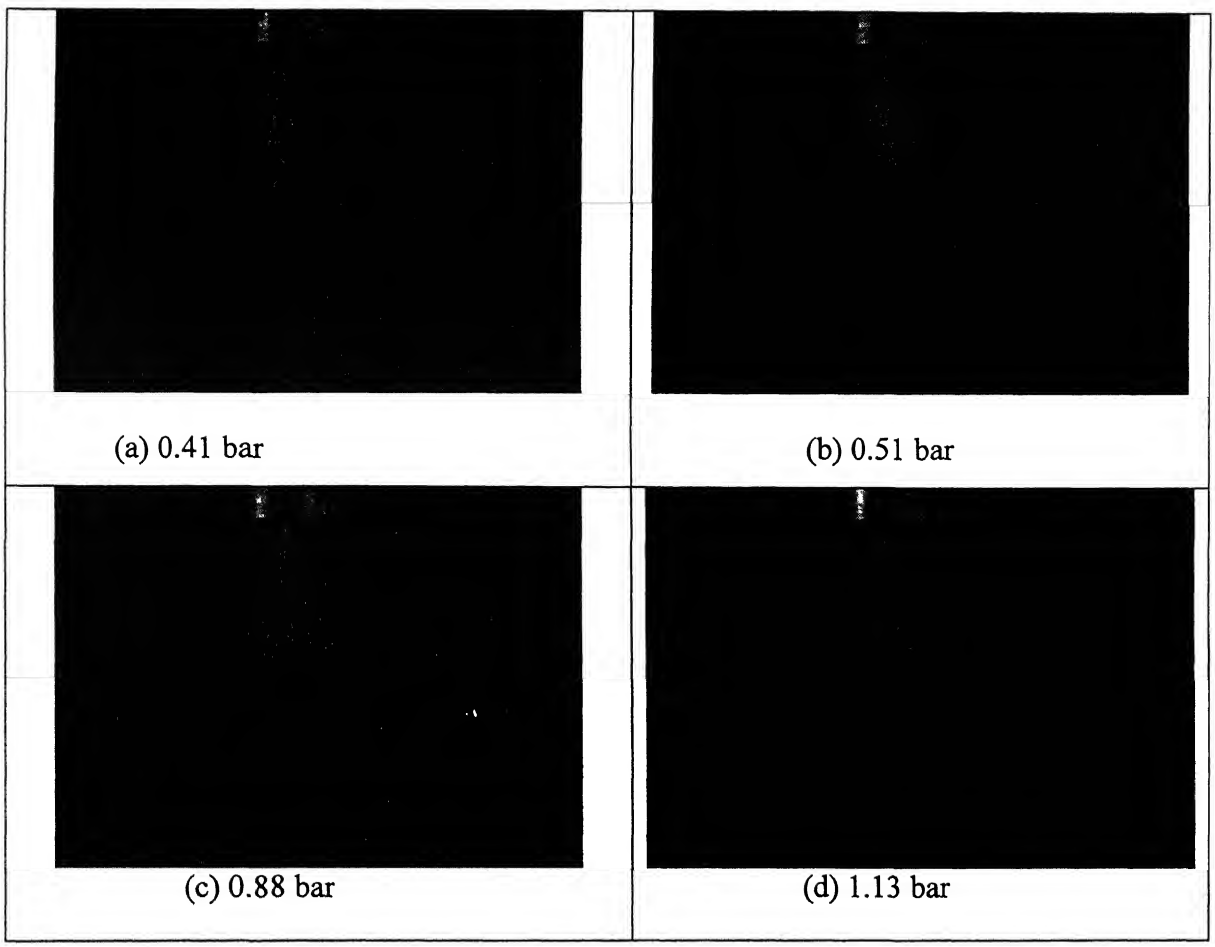

(a) 0.41 bar

(b) 0.51 bar

(c) 0.88 bar

(d) 1.13 bar

(e) 1.48 bar

(f) 1.8 bar

(g) 2.17 bar

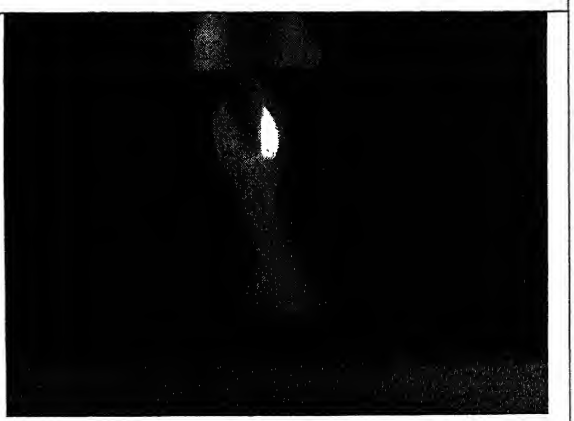

(h) 2.58 bar

(i) 3 bar

(j) 3.44 bar

(k) 3.96 bar

(l) 4.96 bar

(m) 5.96 bar

(n) 6.16 bar

(o) 6.75 bar

(p) 7.55 bar

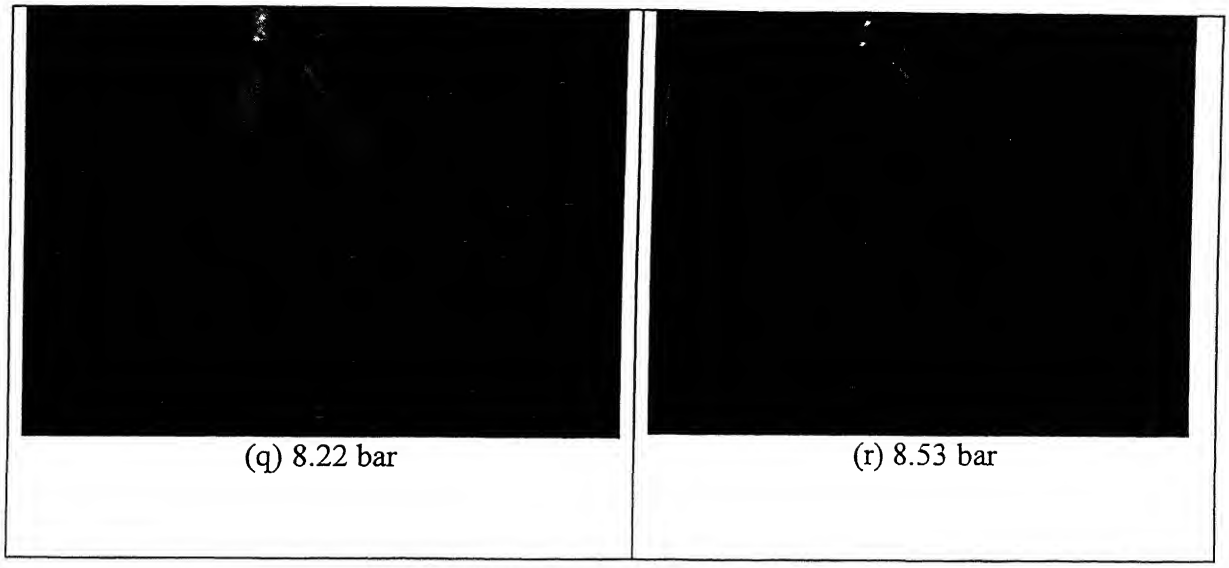

(q) 8.22 bar (r) 8.53 bar

Figure 5.1 Evolution of spray in pressure-swirl Atomizer.

Figure 5.2 shows the dependence of velocity on pressure. As pressure increases velocity increases according to the equation $\left(V = \sqrt{\frac{2\Delta P}{\rho}}\right)$.

Figure 5.3 Shows the dependence of Reynolds number ($R_e = \frac{\rho V d_2}{\mu}$) on pressure. As pressure is increased, velocity is increased and hence, the inertial force, and is so the Reynolds number. Because only one type of fluid i.e. water was used as experimental liquid, the density and viscosity remain constant (temperature is constant so viscosity and density are also constant because viscosity and density are negligibly affected by pressure as water is incompressible fluid).

Figure 5.4 and 5.5 show the dependence of actual co-efficient of discharge ($C_{da}$) on non-dimensional pressure ($\Delta P/P_{atm.}$) and Reynolds number. The value of Reynolds number based on minimum pressures of 0.28 bars is 5486.4. So the flow is already turbulent. For turbulent flow $\mathbf{C_{da}}$ should be independent of Reynolds number ($R_e = \frac{\rho V d_2}{\mu}$) [11]. But from experimental result it was found that the even though the flow is initially turbulent $\mathbf{C_{da}}$ is tending to be constant at higher $R_e$ i.e. $R_e$=20000. At this

value of $R_e$ bulb is opened and the air core is fully developed. For pressure-swirl atomizer it can be concluded that $\mathbf{C_{da}}$ is not a function of $R_e$ only but also gas Weber number (We) i.e. surface tension will affect $\mathbf{C_{da}}$ until the air core is fully developed. Possible explanation for gradual small decrement of $\mathbf{C_{da}}$ unto $R_e$=20000 is gradual development of air core in the orifice and consequent generation of surface. In order to generate new surface molecular force among the molecules has to be overcome to generate that surface and the energy requirement for doing that is called surface energy. This extra surface energy is being supplied by increased pressure drop. Apart from that, when air core is developing a molecular force gradient between the air molecules and water molecules is also established giving rise to surface tension force. This force gradient is also has to be overcome at the expense of increased pressure drop. When the air core is fully developed the total surface generated in the orifice, spin chamber and settling chamber is constant, so the energy requirement because of surface tension and new surface generation becomes constant.

The value of $\mathbf{C_{da}}$ **=0.17,** obtained experimentally for fully developed air core for $R_e$=20000. From theoretical result it has been concluded that the magnitude of co-efficient of discharge is a function of non-dimensional geometric characteristics which is 1.57 for this particular injector for $A_S$ =1.57, co-efficient of discharge should be equal to 0.28. The deviation of experimental co-efficient of discharge from that of theoretical value arises because of followings:

1. Fluid friction loss in the helical passage.
2. Secondary flow losses in the helical passage.
3. Friction loss within the fluid itself.
4. Fluid friction loss in the settling chamber.
5. Friction loss in the spin chamber as well as in the orifice passage.

Figure 5.6 shows the dependence of spray angle ($\alpha$) on Reynolds's number. The spray angle was calculated at different points on the surface of the cone and the average value are plotted is shown in figure 5.6. The mean standard deviation in the measurements of the angle is equal to ($\pm$ 7%). It is evident from the plot that as $R_e$

increases (i.e. inertia force both in tangential and axial direction increases) spray cone angle increases and it becomes constant at $R_e$ =20000. Further increase in $R_e$ beyond 20000 cannot increase spray angle. It is because at this $R_e$ bulb is opened and the air core is fully developed. From theoretical analysis it has been proved that for fully developed air core, spray angle is dependent of only non-dimensional geometric characteristic and independent of liquid supply pressure i.e. Reynolds' number. So theoretically predicted spray angle is quite correct. But theoretically predicted cone angle is 88.5 degree which is more than experimentally found value by 8.5 degree. This 8.5 degree takes care of real flow effect in the injector

Figures 5.7 and 5.8 show dependence of $W_e$ on velocity and non-dimensional supply pressure and are self-explanatory.

Figure 5.9 and figure 5.10 explain the dependence of non- dimensional sheet break-up length ($l/d_2$) (average each) on the non-dimensional liquid supplied pressure and Gas Weber number. Both the plots show that the non-dimensional break-up length first decreases and then increases at point where the air core is fully developed at Weber number ($W_e$) =7.45. After the air core is fully developed, the sheet break-up length start decreasing and it may be decreased to zero break-up length depending upon the pressure and corresponding Weber number.

In both the plots the total break up process can be divided into three stages and the possible explanation are give below.

First Stage: Up to a pressure of 0.41bar and corresponding Weber number of 0.892 the air core yet is to be established. It is not Reyleigh break up. Because already flow is turbulent in the orifice and the minimum velocity corresponding to pressure 0.28 bar is 7.856 m/s. As per as Reyleigh break is concerned with very low velocity, the first stage should be due to rotationally symmetric oscillation with additional effect of air friction.

Second Stage: Second stage is terminated by the opening of the bulb at a pressure of 3.44 bars and corresponding Weber number 7.48 and Reynolds number of 20000. In this stage the sheet breaks up through waviness of the jet, assisted by air friction with additional

effect of inner surface generation because of gradual development of air core due to more swirling motion. This inner surface due to air core will give extra compactness to the sheet owing to surface tension property of the liquid and will delay the break up process. In this stage final break up occurs due to mutual impingement.

Third Stage: Disintegration of liquid sheet is promoted by swirling motion as well as turbulence and by the action of air forces on the surface of the sheet. This three main forces are opposed by the viscosity and surface tension forces of the liquid which tend to preserve the continuous and compact state of the sheet. Hence, when pressure as well as Weber number is increases beyond bulbs opening break up length, it starts decreasing with consequent higher degree of atomization.

The results shown in this section are in agreements with the behavior of swirling jet break up regime described by (11)

These results can be used to orient the fuel injector inside a combustor to obtain optimum dispersion of fuel inside the combustor with settling the combustor surface and thus, increasing the efficiency.

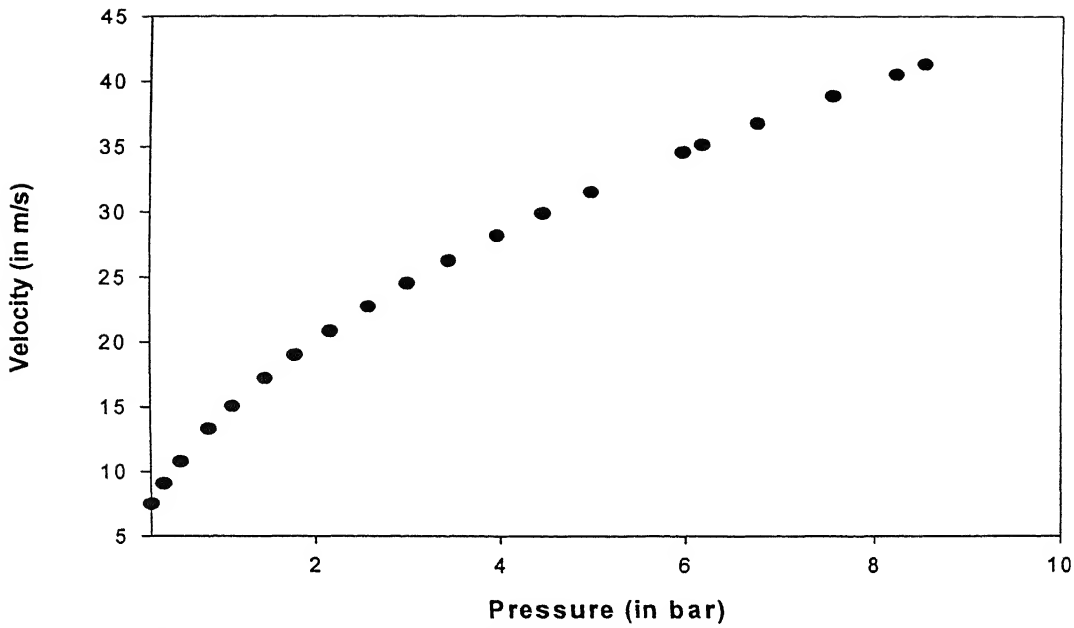

Figure 5.2 Dependence of velocity on pressure.

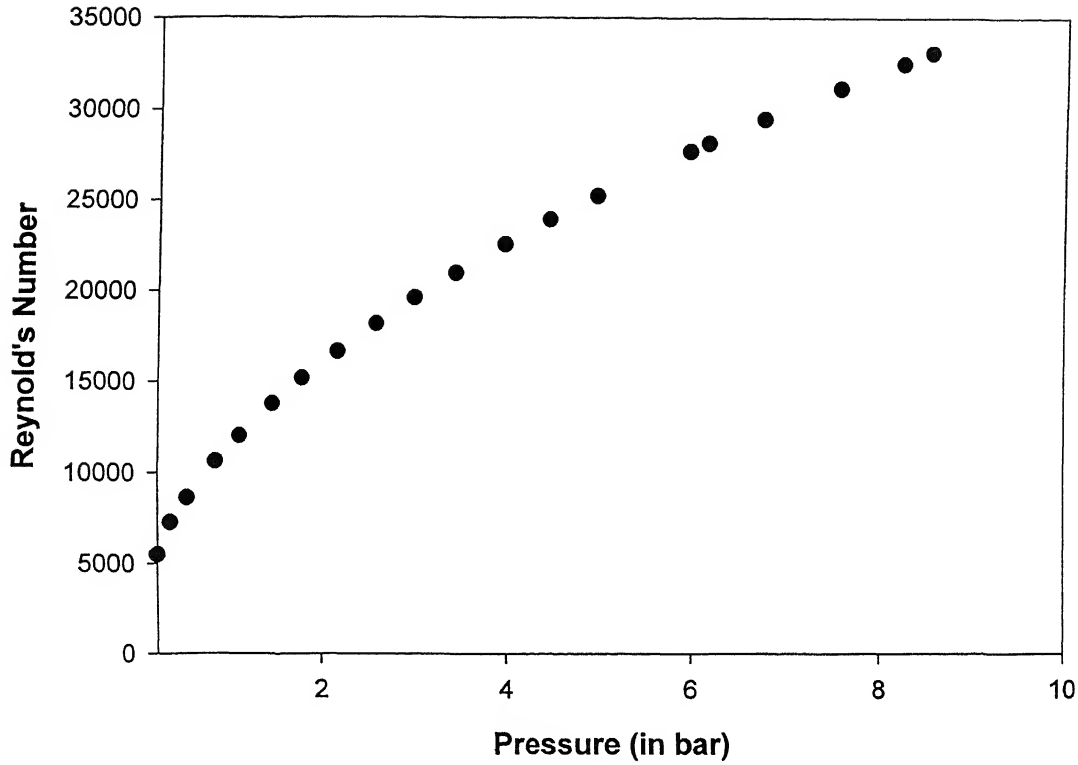


Figure 5.3 Dependence of Reynolds number ( $R_e = \frac{\rho V d_2}{\mu}$ ) on pressure.

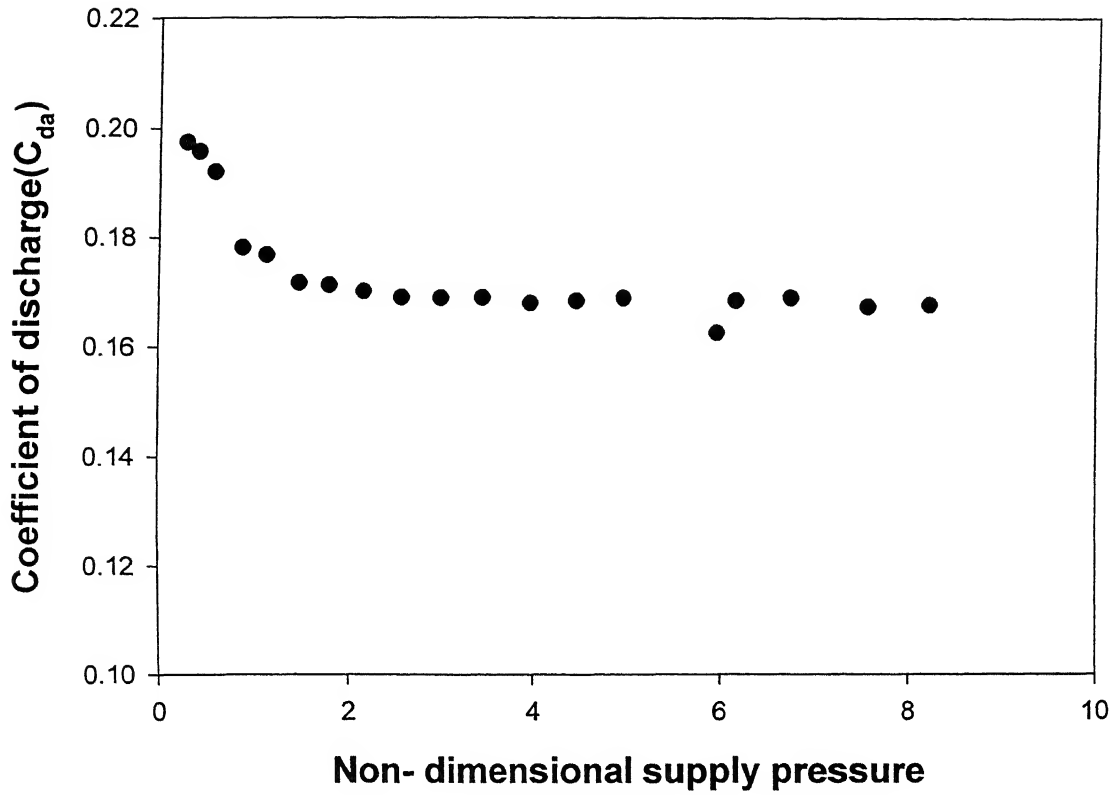


Figure 5.4 Dependence of Co-efficient of discharge ($C_{da}$) on non-dimensional pressure.

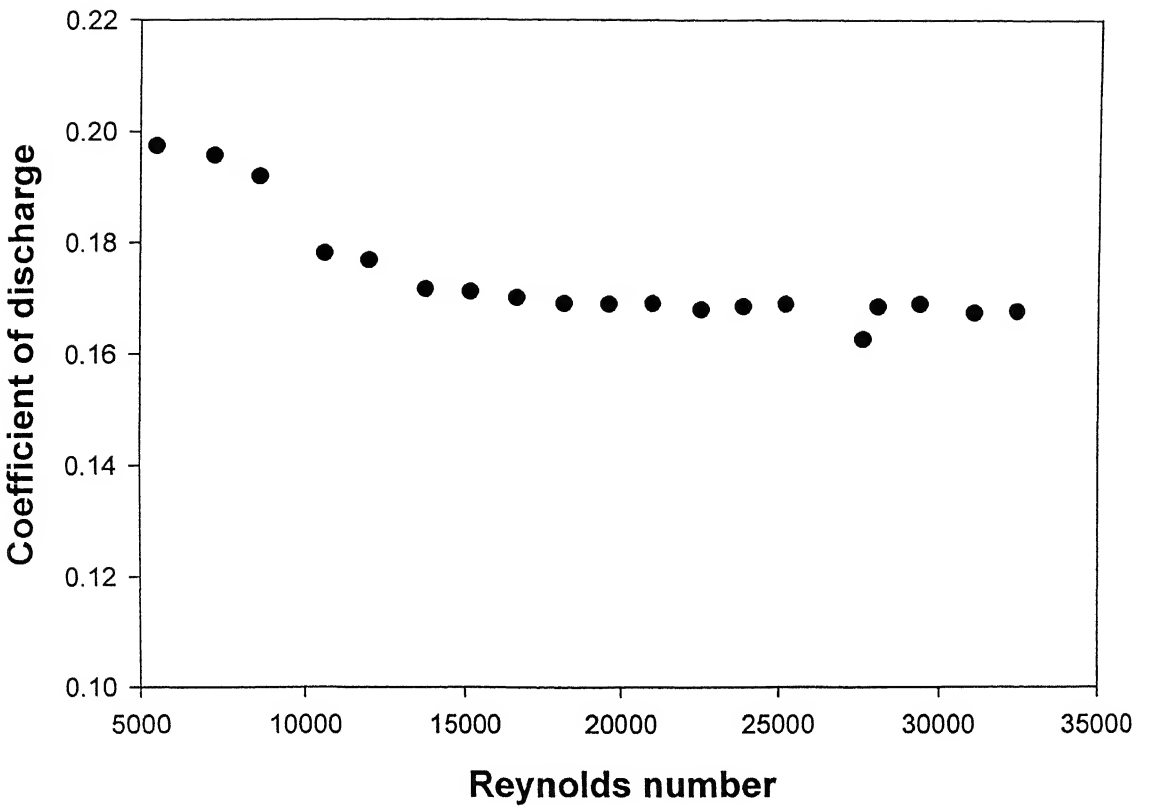


Figure 5.5 Dependence of Reynolds number on the actual co-efficient of discharge ($C_{da}$)

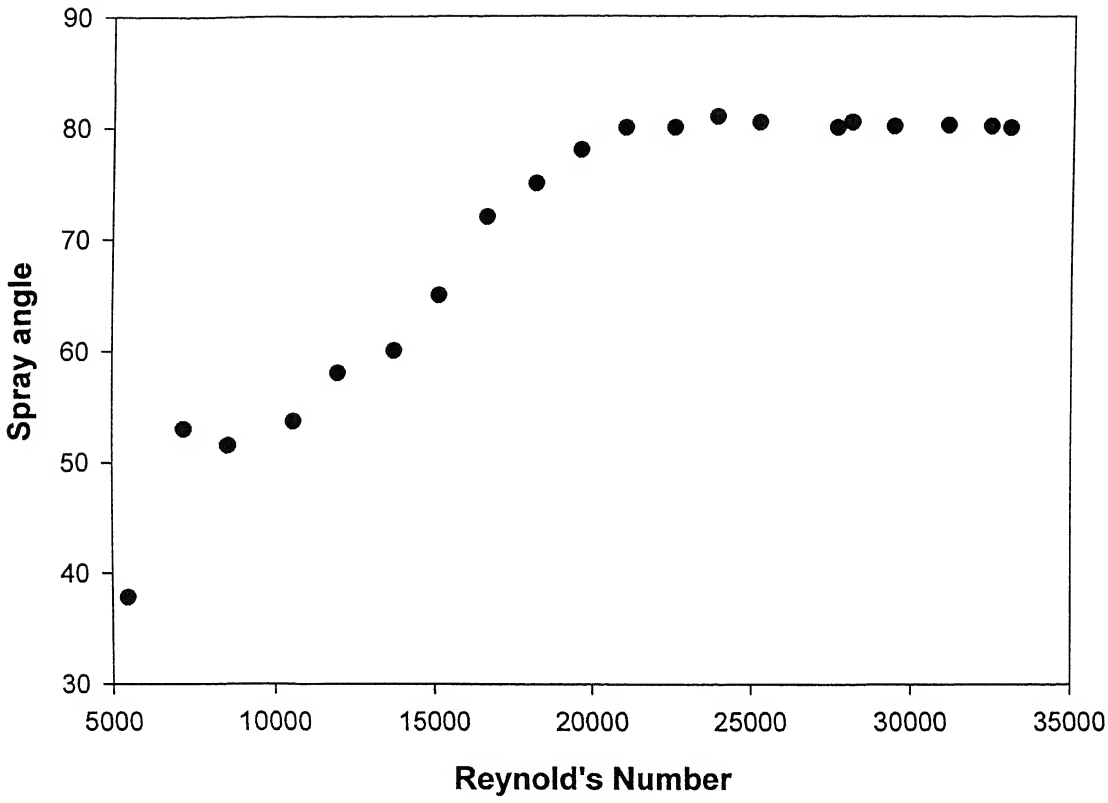


Figure 5.6 Dependence of spray angle on Reynolds's number

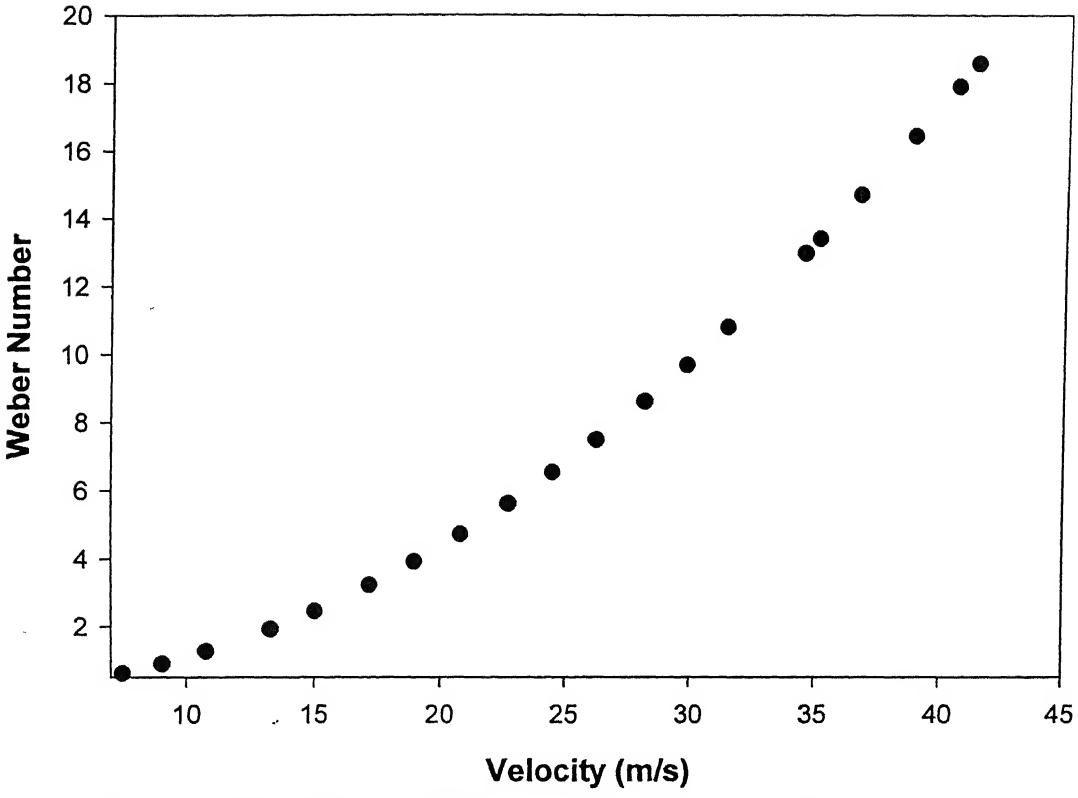

Figure 5.7 Dependence of Weber number ($W_e$) on velocity.

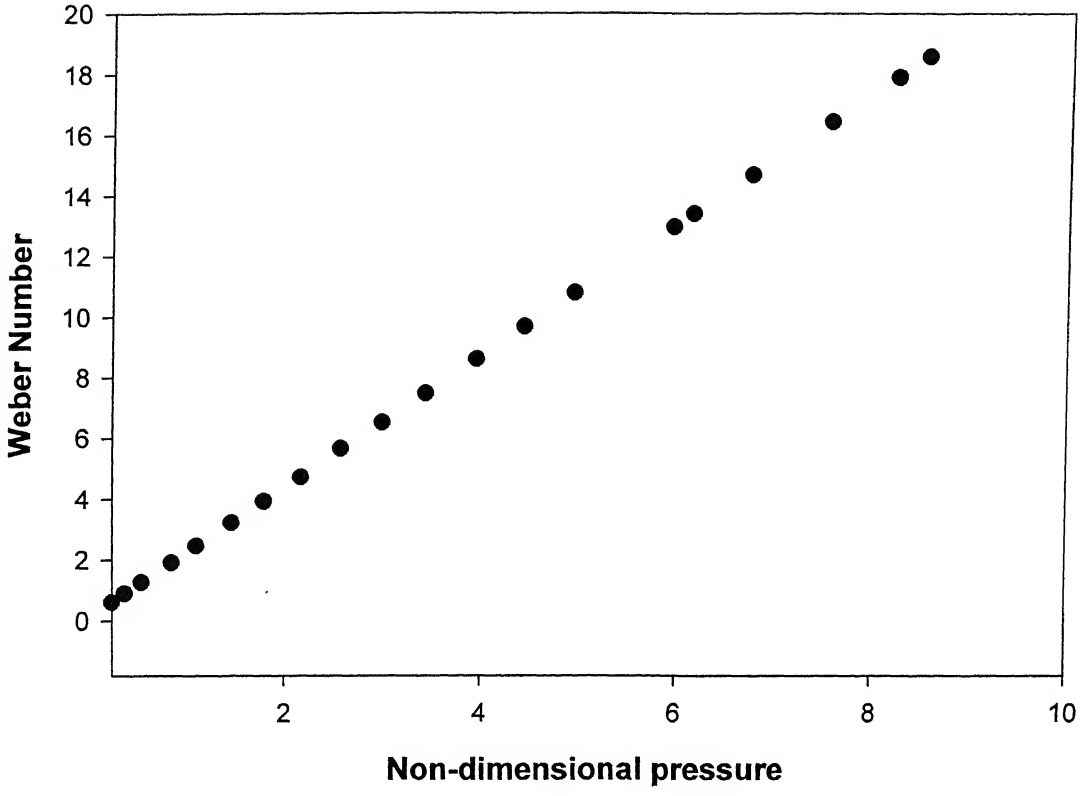


Figure 5.8 Dependence of Weber number ($W_e$) on non-dimensional pressure.

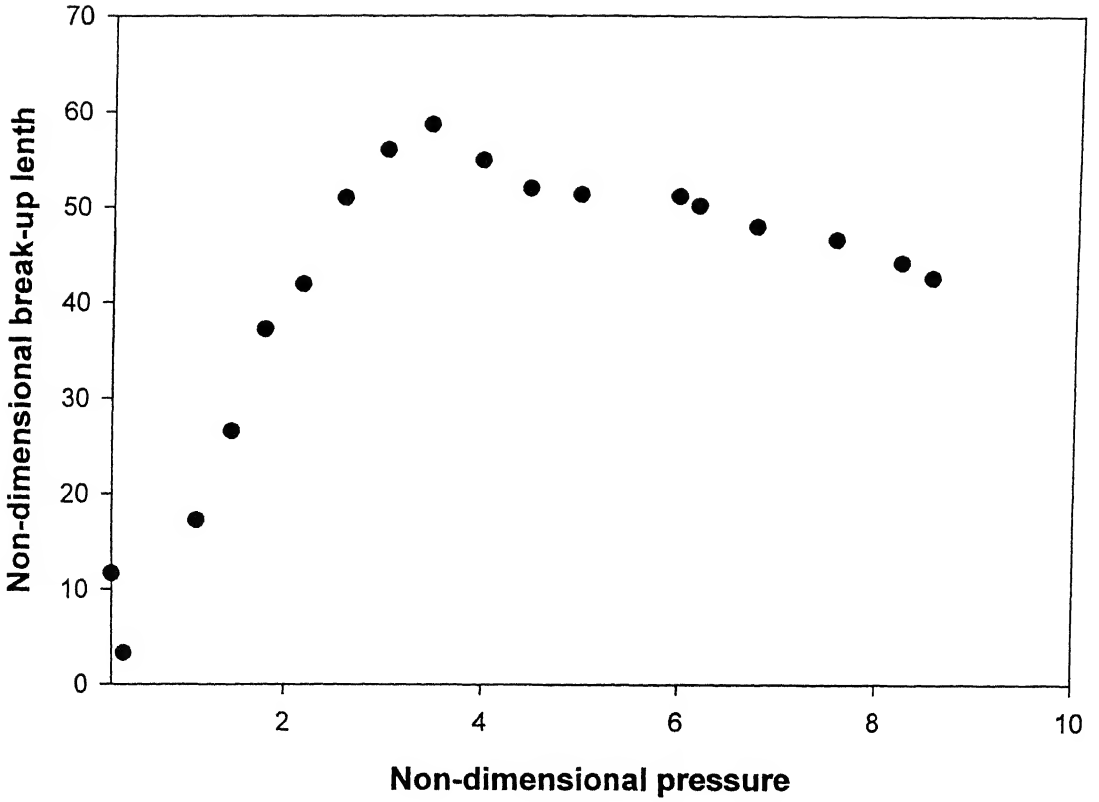


Figure 5.9 Dependence of non-dimensional break up length on non-dimensional pressure.

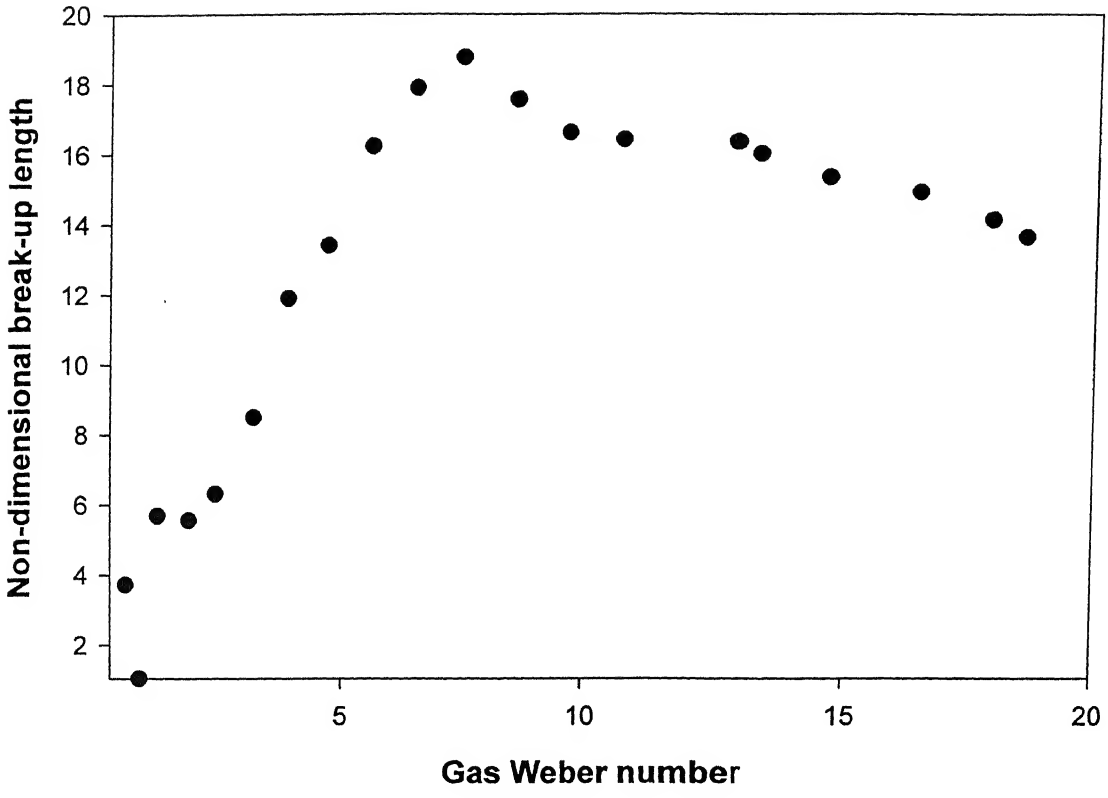


Figure 5.10 Dependence of non-dimensional break up length on Gas Weber number.

# CHAPTER VI

## Conclusions

Helical passage pressure-swirl atomizer has been investigated theoretically and experimentally and the results are compared. It has been seen that the theoretical prediction are in agreement with the experimental values. The deviation between the theoretical and the experimental values is due to real flow effects i.e. viscosity, surface tension and secondary flow effect in the atomizer. Experimentally it has been found that co-efficient of discharge decreases first up to bulb opening length and then becomes constant irrespective of liquid supply pressure i.e., co-efficient of discharge becomes independent of liquid supply pressure and is only the function of non-dimensional geometric characteristics.. At this point and after the bulb opening point, the air core in the atomizer becomes fully developed, so the surface tension effect arising from internal surface generation becomes marginally constant. The jet break up length first decreases because of rotationally symmetric oscillations with additional effect of air force friction. Then again sheet break up length start increasing due to internal surface (due to air core) generation which gives compactness and strength to the sheet. Apart from this at this stage break up is delayed by the waviness of the jet assisted by air force. Up to the opening of the bulb, the break up is premature due to mutual convergence of the sheet. As soon as bulb is opened and air core is fully developed break up length starts decreasing. This is because of increased tangential velocity and increased inertial forces which overcome the consolidating influence of surface tension and non-disrupting influence of viscosity.

# References


1. N. K. Rizk and A. H Lefebvre, "Internal Flow Characteristics of Simplex Swirl Atomizer," Journal of Propulsion and Power, vol.1, No3, 1985, pp. 193-199.
2. M. Suyari and A. H Lefebvre, "Film Thickness Measurements in a Simplex Swirl Atomizer," Journal of Propulsion and Power, vol.1, no. 6, 1986, pp. 528-533.
3. E. Giffen and A. Muraszew, The Atomization of Liquid Fuels, Chapman and Hall Ltd., London, 1953.
4. A. H. Leferve, "Fuel effects on gas turbine combustion – ignition, stability and Combustion efficiency", ASME J.Engg.Gas Turbines and Power, vol.107, pp.24-37, 1985.
5. K. K.Rink and A.H. Leferve, "Pollutant formation in heterogeneous mixtures of fuel drops and air", AIAA J.Propulsion, vol.3 No. 1, pp. 5-10, Jan-Feb, 1987.
6. A. H Leferve, Gas Turbine Combustion, McGraw Hill, New York, 1983.
7. A. H. Lefeve, Atomization and spray, Hemishere Publishing Corporation, 1989.
8. J. S. Chin, "Effervescent atomization and internal mixing air assisted atomization", Int. J. of Turbo and Jet Engines, 12, pp. 119-127, 1995.
9. J. S. Chin and A. H. Leferve, "A design procedure for effervescent atomizers", ASME J. of Engineering for Gas Turbines and Power, vol. 117, pp. 266-271, April 1995.
10. T. Sakai, M. Kito, M. Saito and T. Kanbe, "Characteristics of Internal mixing twin-fluid atomizer", Proceeding of the 1st International Conference on Liquid fluid atomization and Spray Systems, Tokyo, August 1978, Paper 10-1, pp. 161-168, 1978.
11. M. N. Biswas, "Atomization in two-phase critical flow", Proceeding of the 2st International Conference on Liquid fluid atomization and Spray Systems, (ICLASS-82), pp. 145-151, 1982.
12. A. Kushari, Y. Nuemeier, O. Israeli, A. Peled and B.T. Zinn," An Internally mixed injector for active control of atomization process in liquid fueled engines",

AIAA 99-0329, 37th AIAA Aerospace Scienece Meeting and Exhibit, Jan. 11-14, 1999, Reno, NV.

13. X. Li, "Spatial instability of plane liquid sheets", Chemical Engineering Science, vol. 48, No. 16, pp. 2973-2981, 1983.
14. W. G. Pritchard, "Instability and chaotic behavior in a free-surface flow", J. Fluid Mech., vol. 165, pp. 1-60, 1986.
15. G. Biswas, S. K. Som, A. S. Gupta, "Instability of moving cylindrical liquid sheet", ASME J. of fluid Engineering, vol. 107, pp. 451-454, Dec. 1985.
16. G .D. Crapper, N. Dombrowski, "A note on the effect of forced disturbances on the stability of thin liquid sheets and on the resulting drop size", Int. J. of Multiphase Flow, vol. 10, No. 6, pp. 167-169,1953.
17. C. J. Clark and N. Dombrowski, "Aerodynamic instability and disintegration of inviscid liquid sheets", Proc. R. Soc. Lond. A. 329, pp. 467-478, 1972.
18. R. D. Reitz and F.V. Bracco,"Mechanism of atomization of a liquid jet", Phys. Fluids, 25, 1730, 1982.
19. Lord Rayleigh, The Theory of Sound, Dover Publications, NY 1945.
20. C. Weber, "Disintegration of Liquid jets", Z. Angrew. Math. Mech.,vol.11, no. 2, pp. 136-159, 1931.
21. C. A. Spangler, J. H. Hilbing and S. D. Heistar, "Non linear modeling of jet atomization in wind induced regime", Phys. Fluids, vol. 7(11), pp. 2915-2917, Nov. 1995.
22. A. Kushari et al., "Internally Mixed Liquid Injector for Active Control of Atomization Process", AIAA J. of Propulsion and Power, vol. 17, No. 4, pp. 878-882, July-August 2001.
23. A. Kushari, "Design and Investigation of Helical Injector", B.Tech. Thesis in Engineering submitted to Dept. of Aerospace Engg., I.I.T, Kharagpur, 1994
24. A. Kushri, "Study of an Internally Mixed Liquid Injector for Active Control of Atomization Process", Ph.D Thesis in Engineering submitted to Dept. of Mechanical Engg., Georgia Institute of Technology, Atlanta, 2000.
25. A. A. Shraiber, A. M. Padysotsky and V. V. Dubrovsky, "Deformation and break up of drops by Aerodynamic forces", Atomization and Sprays, vol. 6, pp. 667-

692, 1996.

26. R. Bruce, Donald F. Munson. Young and H. Theodore Okiishi, Fundamentals of Fluid Mechanics, John Wiley & sons, inc. 1940.
27. M. L Mathur and R. P Sharma, Internal Combustion Engines, Dhanpat rai & sons, 1976.
28. H. Cohen, G. F. C Rogers and H. I. H. Saravanamuttoo, Gas Turbine Theory, Longmn, 1972.
29. C. M. Reeves and A. H. Leferve, "Fuel effects on aircraft combustor emissions", ASME(paper), 86-GT-212,1986.
31. I-Ping Chung and Cary Presser, "Fluid Property Effects on Sheet Disintegration of a Simplex Pressure-swirl Atomizer", AIAA J. of Propulsion and Power, vol. 17, No. 1, Jan-Feb., 2001.
31. G. Biswas, S. K Som A. S Gupta, "Instability of a moving cylindrical liquid Sheet", ASME J. of Fluids Engineering, vol.107, pp.451-454, Dec.1985.